**UNIVERSITÀ DEGLI STUDI**

**DI GENOVA**

Doctoral School in “Neuroscience”

Curriculum “Clinical and Experimental Neuroscience”

XXXIV cycle

# "Role of the novel neuronal protein APache in autophagy"

Candidate: **Barbara Parisi**

Supervisor: **Silvia Giovedì**

# Table of contents

# Abstract

The central event driving neuronal activity is represented by synaptic transmission, a process that relies on regulated cycles of synaptic vesicle (SV) exocytosis and endocytosis at presynaptic terminal level. Neurons, polarized and perennial cells, to guarantee an efficient neurotransmitter release, to maintain cellular homeostasis and promote neuronal survival, are particularly dependent on efficient quality control pathways to continuously remove dysfunctional presynaptic proteins and organelles. The main mechanisms used by neurons to achieve these goals are endosomal sorting and autophagy, a highly conserved endo-lysosomal degradation pathway required to recycle basic nutrients by the clearance of damaged or aged proteins and organelles.

Several presynaptic endocytic proteins have been shown to regulate both SV recycling and autophagy and defects in both pathways have been linked to neurodevelopmental abnormalities and neurodegeneration in mouse and humans.

In 2017 we characterized the previously unknown protein APache (KIAA1107) as a neuronal-specific protein, novel interactor of the adaptor protein AP-2 essential in the regulation of neuronal development and SV cycle *in vitro* and *in vivo*.

In this work, we intended to define APache functional role in neuronal autophagy by combining electron microscopy, immunofluorescence, live-cell imaging microscopy and biochemistry. We observed that APache is actually involved in autophagy: the induction of the process increases APache levels in mature neurons and, conversely, APache silencing leads to a severe accumulation of late-stage autophagosomes in neurons, also at synaptic level, due to autophagic blockade. Interestingly, APache expression is significantly reduced in the brain of sporadic Alzheimer's disease patients.

These data point to APache as a novel key regulator of neuronal autophagy. Its altered levels, resulting in defective autophagy, may contribute to the precocious cellular alterations and synaptic dysfunctions observed in neurodegenerative diseases. The further elucidation of its functional role in neurons and of its precise molecular mechanism will help our understanding of the physiology and pathology of synaptic function.

# List of abbreviations

| | |
|---|---|
| **AD** | Alzheimer Disease |
| **ADBE** | activity-dependent bulk endocytosis |
| **AP-2** | assembly protein complex 2 |
| **APache** | AP2-interacting clathrin-endocytosis protein |
| **APP** | amyloid precursor protein |
| **ATG** | autophagy-related gene |
| **AV** | Autophagic vacuole |
| **AZ** | active zone |
| **Aβ** | β-amyloid |
| **BACE1** | β-site APP cleaving enzyme 1 |
| **BDNF** | brain-derived neurotrophic factor |
| **CCP** | clathrin-coated pit |
| **CCV** | clathrin coated vesicle |
| **CMA** | chaperon-mediated autophagy |
| **CME** | clathrin mediated endocytosis |
| **CTSD** | cathepsin D |
| **DIV** | days in vitro |
| **E** | embryonic day |
| **ELV** | endosome-like vacuole |
| **LAMP1** | lysosomal-associated membrane protein 1 |
| **LAMP2** | lysosomal-associated membrane protein 2 |
| **LC3** | microtubule-associated protein 1 light chain 3 |

| | |
|---|---|
| **MBV** | multivesicular body |
| **MOI** | multiplicity of infection |
| **mTOR** | mammalian target of rapamycin |
| **NaK3** | $Na^+/K^+$ ATPase α-3 |
| **NFT** | neurofibrillary tangles |
| **NT** | neurotransmitter |
| **P** | postnatal day |
| **p38** | synaptophysin |
| **p62** | see “SQSTM1” |
| **PAS** | pre-autophagosomal structure |
| **PE** | phosphatidylethanolamine |
| **PI2P** | phosphatidylinositol-4,5-bisphosphate |
| **PI3KC3** | class III phosphatidylinositol 3-kinase |
| **PI3P** | phosphatidylinositol 3-phosphate |
| **ShRNA** | short hairpin RNA |
| **SNARE** | soluble NSF attachment protein receptors |
| **SQSTM1** | sequestosome 1 |
| **SV** | synaptic vesicles |
| **Syn I** | synapsin I |
| **Syt 1** | synaptotagmin 1 |
| **TOR** | target of rapamycin |
| **TrkB** | tropomyosin receptor kinase B |
| **Ub** | ubiquitin |
| **UFE** | ultrafast endocytosis |
| **ULK1** | Unc-51- like kinase 1 |
| **UPS** | ubiquitin-proteasome system |
| **VAMP2** | vesicle associated membrane protein 2 |

| | |
|---|---|
| **vATPase** | vacuolate ATPase |
| **VPS34** | see “PI3KC3” |
| **WT** | wild type |

# 1. Introduction

## 1.1 Autophagy

Cell growth and homeostasis depend on the balance between synthetic and degradative processes. In eukaryotic cells, there are two main systems that guarantee a proper turnover of proteins and organelles: the ubiquitin-proteasome-system (UPS), mostly responsible of the degradation of short-lived or misfolded soluble proteins (Ciechanover and Brundin, 2003; Inobe and Matouschek, 2014), and the lysosomal system (Knecht et al., 2009), involved in the turnover of larger structures, such as integral membrane proteins, protein aggregates and organelles (Johansen and Lamark, 2011; Lilienbaum, 2013).

The UPS starts with an enzymatic cascade that leads to the proteolytic cleavage of the ubiquitin (Ub) precursor, with its consequential activation and attachment to the target protein. Ub-tagged proteins get delivered to the proteasome, a large protein complex where the substrate get degraded by several hydrolases, permitting the recycling of its basic components (Tanaka, 2009; Livneh et al. 2016).

Lysosomal clearance is mediated by two different pathways strongly interconnected: endocytosis, responsible for the degradation of mostly extracellular constituents, and autophagy, a degradative system for intracellular clearance of protein aggregates and defective organelles (Levine and Klionsky, 2004; Mizushima, 2007).

Autophagy is a highly conserved self-eating process essential to obtain basic metabolites during stress or starvation. In addition, autophagy occurs also at constitutive basal level and represents a highly selective quality control system that prevents cell damage by recycling old or damaged cell components. Thus, autophagy results crucial to regulate cell survival and homeostasis (Klionsky and Emr, 2000; Debnath et al., 2005; Reef et al., 2006).

Autophagy can be classified in three distinct types, that differ in cargo recognition and capturing: chaperon-mediated autophagy (CMA), highly specific and based on the direct transport of target proteins to the lysosome and consequential unfolding by chaperons, microautophagy, in which cargoes are directly engulfed in lysosomes by lysosomal membrane invagination, and macroautophagy, that occurs by sequestrating

cargoes in double-membranous structures, named autophagosomes, delivered to lysosomes for degradation (Parzych and Klionsky, 2014). The best studied and characterized pathway is macroautophagy.

### 1.1.1 Macroautophagy

Macroautophagy (hereafter referred to as autophagy) is the most efficient and complex type of autophagy. This degradative pathway is regulated by autophagy-related (*ATG*) genes coding the Atg protein group. Due to its crucial role in cell survival and homeostasis, autophagy is highly conserved through evolution. In fact, several Atg proteins, that have been discovered in yeast *S. cerevisiae* (Tsukada and Ohsumi 1993), have homologs in more complex eukaryotes (Yang and Klionsky, 2010), mammalians included. The majority of Atg proteins participate to the formation of the key structure of autophagy, the autophagosome, a double-membrane vesicle that sequesters the target cargo and mediates its transport and fusion to lysosomes. This process can be divided into the following stages characterized by the participation of different adaptors: initiation, autophagosome formation, elongation, enclosure, maturation, and degradation (**Fig. 1**) (Wang and Klionsky, 2003; He and Klionsky, 2009; Nixon, 2013; Lamb et al., 2013).

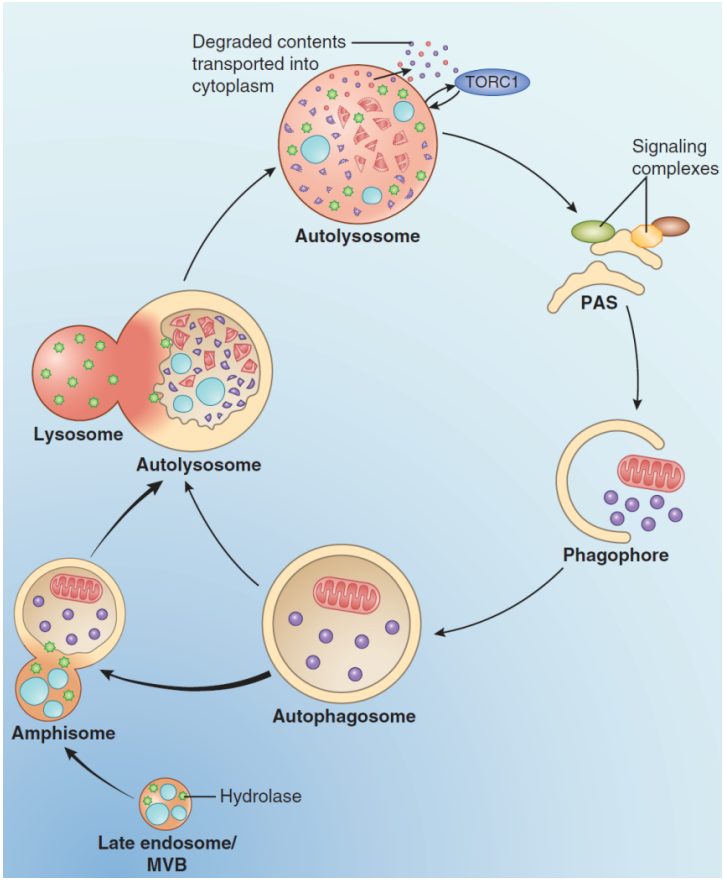

**Figure 1: Schematic overview of macroautophagy (autophagy).**

Autophagy is a complex degradative pathway that allows the turnover of old or damaged cell components and protein aggregates, and can occur selectively or nonselectively. Autophagy is inducted by multiple signaling and by the participation of several adaptor Atg proteins (initiation phase), and starts with the formation of the pre-autophagosomal structure (PAS) (formation phase). PAS evolves in a phagophore or isolation membrane, which expands surrounding the selected substrates (elongation phase). Once the elongating membranes meet, they fuse closing a bilayer autophagosome containing the substrate (enclosure phase). Autophagosomes are delivered to lysosomes and during the journey may fuse with late endosomes or multivesicular bodies (MVB) to form amphisomes (maturation phase). Once autophagosome reaches the lysosome, the two organelles fuse forming the autolysosome (degradation phase). *Image reprinted from Nature Medicine, Vol. 19, Number 8, R.A. Nixon, The role of autophagy in neurodegenerative disease, Pages 983-97, Copyright 2013, with permission from Springer.*

**Initiation** – The key factor that initiates autophagic biogenesis is the activation by dephosphorylation of the Unc-51- like kinase 1 (ULK1), mammalian homologues of yeast Atg1. The main autophagic modulator is the target of rapamycin (TOR; in mammals mTOR), a conserved serine/threonine kinase involved in regulation of cell growth and metabolism (Jung et al.,2010; Inoki et al, 2012). Active TOR interacts with several effectors forming the signaling TOR complex 1 (TORC1), that binds and phosphorylates ULK1, inhibiting its activity and repressing autophagy. Upon nutrient depletion or stress, TOR gets deactivated and dissociates from ULK1, promoting ULK1 activation and autophagy induction (**Fig. 2**) (Kraft et al., 2012; Wong et al., 2013; Wang and Zhang, 2019).

ULK1 activation triggers a phosphorylation cascade that culminates with the assembly of a multiprotein machinery, the ULK complex, at level of the so called pre-autophagosomal structure (PAS) (**Fig. 2**) (Suzuki and Ohsumi, 2010).

**Formation** – Autophagosome formation starts at PAS with the coalescence of small membranous vesicles that form a small bowl-shaped structure called phagophore or isolation membrane. The origin of membranes is still controversial; however, some studies identify the endoplasmic reticulum as the main source (Zhao and Zhang, 2019). At the beginning of nucleation, active ULK1 phosphorylates Beclin-1, the mammalian homolog of Atg6: this event induces the assembly of the class III phosphatidylinositol 3-kinase (PI3KC3, also known as VPS34) complex, where Beclin-1 represents the core component (**Fig. 2**). PI3KC3 complex produces PI3P, a signaling lipid required for recruitment of Atg proteins needed for the subsequent phases of autophagosome initiation (Wirth et al., 2013; Nazarko and Zhong, 2013).

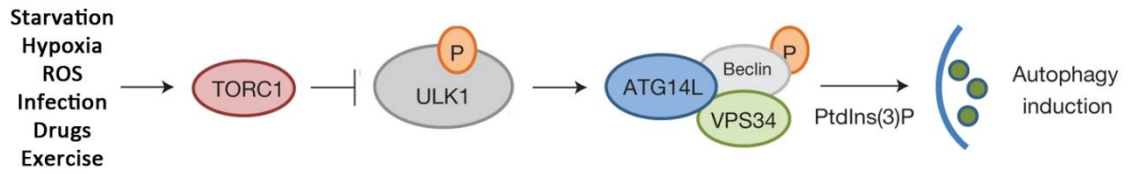


**Figure 2: Model of autophagic induction.**

Upon starvation, stress or specific treatments, the activity of the autophagy inhibitor TOR complex 1 (TORC1) get repressed, causing the de-repressing of ULK1. Active ULK1 triggers a phosphorylation cascade that culminates with the assembly of the class III phosphatidylinositol 3-kinase (PI3KC3, also called VPS34) complex, that includes Beclin-1. VPS34 complex produces the signaling lipid PI3P, and the consequential recruitment of Atg proteins leads to autophagosome initiation. *Image modified from Russell et al., 2013.*

**Elongation and enclosure** – After nucleation, the phagophore begins to expand at both ends (elongation phase), surrounding a portion of the cytoplasm containing the target substrates and sequestering them. Once the ends of the phagophore meet, the membranes fuse, closing a fully formed autophagosome containing the cytoplasmic cargo (Nixon, 2013; He and Klionsky, 2009).

Elongation requires the participation of several SNARE proteins and is achieved through two ubiquitin-like reactions: the formation of the Atg12-Atg5 complex (Mizushima et al., 2020), and the lipidation of Atg8, in mammals protein microtubule-associated protein 1 light chain 3 (LC3) (Hemelaar et al., 2003). Currently, three forms of LC3 are described in literature, with distinct subcellular localizations: LC3A, LC3B and LC3C (Koukourakis et al., 2015). Differently by LC3A and LC3C, that are mostly concentrated in the perinuclear and nuclear areas, LC3B in distributed throughout the cytoplasm (Koukourakis et al., 2015), and represent the most studied LC3 form.

LC3B (hereafter referred to as LC3) is usually present in the cytosol in its soluble form LC3 I. Under autophagy induction, LC3 I get conjugated to a phosphatidylethanolamine (PE) in a reaction involving the Atg12-Atg5 complex, Atg7 and Atg3, to form LC3 II (Shpilka et al. 2011; Nakatogawa 2020). LC3 II is specifically targeted to the expanding phagophore and gets bound to autophagic membranes. Unlike other Atg proteins that dissociate from the phagophore, LC3 II remains on autophagosome membranes till lysosomal degradation (Satoo et al. 2009).

LC3 role in autophagy is still matter of debate, however several findings propose that LC3 mediates the closure of autophagic membrane (Longatti and Tooze, 2009). Although LC3 molecular mechanism remains still unclear, the constant association of

LC3 II to the autophagosomes makes it an excellent autophagy-specific marker (Zhang et al., 2013; Mizushima et al., 2020).

Cargo sequestration inside autophagosomes can occur in a non-selective bulk assimilation under starvation (Ryter et al., 2013), or in a selective manner to eliminate Ub-tagged structures. The identification of specific target is mediated by autophagy cargo adaptors, such as sequestosome 1 (SQSTM1, also called p62) (He and Klionsky, 2009; Nixon, 2013), a multidomain receptor that interacts with ubiquitinated substrates and binds them to LC3 II, targeting the cargo inside the enclosing phagophore (**Fig. 3**). During the process p62 itself get engulfed in the autophagosome and get degraded by lysosomes along with the cargo. For this reason, p62 level highly correlates to autophagic activity, representing a useful marker to monitor the autophagic efficiency (Bjørkøy et al., 2009; Zhang et al., 2013; Mizushima et al., 2020).

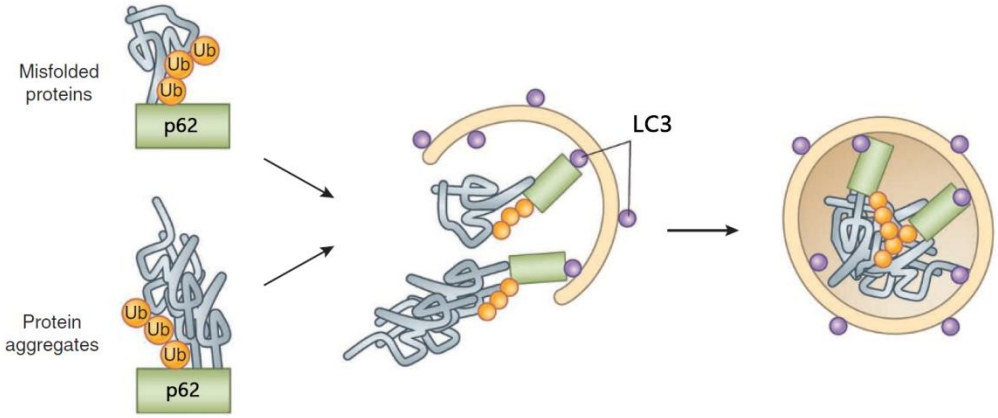


**Figure 3: Selective autophagy mediated by p62.**

Selective autophagy is required for the elimination of ubiquitinated misfolded proteins and protein aggregates. The recognition of Ub-tagged protein is mediated by the receptor sequestosome 1 (SQSTM1, also called p62), that binds them and recruits them to the enclosing phagophore by binding with LC3 II. *Image modified from Nixon et al., 2013.*

**Maturation and degradation** – After membrane enclosure, neo-formed autophagosomes are trafficked along microtubules toward lysosomes (Maday et al., 2012; Maday and Holzbaur, 2014). During this journey mediated by dynein-dynactin motor complex, autophagosomes may undergo to maturation by fusion with late acidified endosomes positive for guanosine triphosphatase Rab7 and the lysosomal-associated membrane protein 1 (LAMP1), forming amphisomes (Maday and Holzbaur, 2016). Eventually autophagosomes/amphisomes fuse with lysosomes to become autolysosomes (Maday and Holzbaur, 2016). The formation of autolysosomes requires the participation of several proteins, such as LC3 II, SNARE proteins, that mediate the

fusion between the two membranes (Yu and Melia, 2017), and endosomal proteins Rab7, LAMP1 and LAMP2 (Huynh et al., 2007; Gutierrez et al., 2004).

The presence of the protonic pump vacuolate ATPase (vATPase) on the lysosomal membrane allows the acidification of the lysosomal lumen to pH~4.5–5.0 (Saftig and Klumperman, 2009; Mindell, 2012; Trivedi et al., 2020), where several hydrolases are contained, in particular members of the chatepsin family (Roberts, 2005¸ Trivedi et al., 2020). The acidic pH promotes hydrolases activity (Mindell, 2012; Trivedi et al., 2020) that degrades both cargo and autophagosome inner membrane, consequentially basic components are released into the cytoplasm through lysosomal permeases for reuse.

### 1.1.2 Neuronal autophagy

Autophagy is essential for neuronal physiology and survival. Neurons are indeed perennial, complex polarized cells subjected to high constant activity, dependent on intracellular trafficking and protein quality control mechanisms to maintain proper homeostasis and sustain their function, particularly at synaptic level (Wang et al., 2013; Wertz et al., 2020). The central event driving neuronal activity is the neurotransmitter (NT) release by fusion of synaptic vesicles (SVs) with the presynaptic membrane (Azarnia Tehran et al., 2018). To guarantee an efficient NT release and promote neuronal survival, dysfunctional presynaptic components must be continuously removed through endosomal sorting and autophagy, highlighting the importance of a proper quality control mechanism at presynaptic level (Wang et al., 2013; Vijayan and Verstreken, 2017). Moreover, neuron-specific depletion of autophagy in mice results in axon degeneration, accumulation of ubiquitin-containing protein aggregates, and neuronal cell death (Hara et al., 2006; Komatsu et al., 2006, 2007). Neuronal morphology, functionality and lifespan are therefore highly dependent on autophagy, that in neurons results constitutively highly active and exhibits an important spatiotemporally regulation proceeding through compartmentalized stages (Maday and Holzbaur, 2016; Kulkarni and Maday, 2018a).

In neurons, autophagy mainly starts with the formation of autophagosomes within presynaptic boutons and is followed by their retrograde transport along axonal microtubules toward the soma, where lysosomes are enriched (**Fig. 4**).

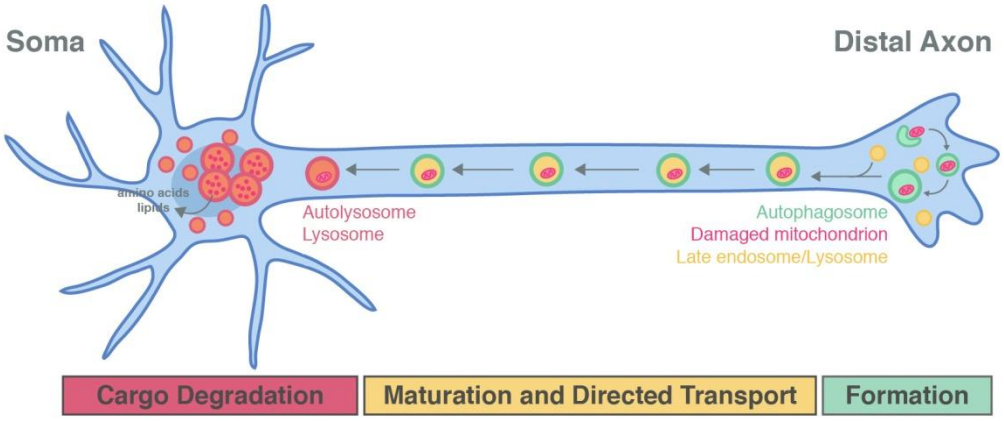


**Figure 4: Schematic representation of autophagic pathway in neurons.**

Neuronal autophagy proceeds in a compartmentalized manner. The pathway starts with the formation of autophagosomes at synapses, and is followed by their retrograde transport along the axon. Finally, autophagosomes reach the soma and fuse with lysosomes. *Image modified from Maday Lab official site, no date; https://www.med.upenn.edu/madaylab/research.html*

Retrograde trafficking is achieved by Snapin and Dynein motor complexes, which autophagosomes acquire by fusion with late endosomes (**Fig. 5**) (Wang et al., 2015; Cheng et al., 2015; Kulkarni and Maday, 2018b; Hill and Colón-Ramos, 2020). During their axonal transport, autophagosomes indeed undergo maturation by fusion with Rab7- and LAMP1-positive late endosomes. Thus, neuronal autophagosomes/amphisomes present a gradient of maturation from the proximal axon to the distal regions, observable by Rab7 and LAMP1 distribution analysis (Cheng et al. 2018; Yap et al. 2018).

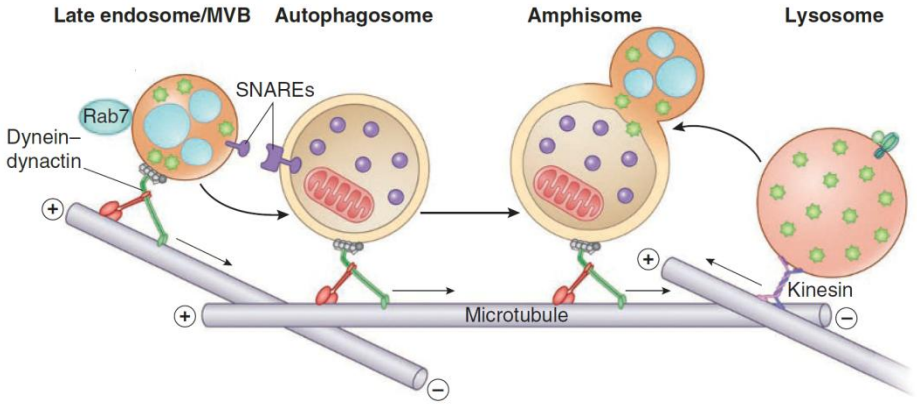


**Figure 5: Overview of autophagic transport.**

Autophagosomes are delivered to the soma by retrograde transport along axonal microtubules mediated by the motor complex dynein-dynactin. During the journey autophagosome may undergo to maturation by fusion with Rab7-positive late endosome or MBV to form amphysomes, process mediated by SNARE proteins. In the end, amphisomes fuse with lysosomes, that may move in anterograde direction via motor complex kinesin, to form autolysosomes. *Image modified from Nixon et al., 2013.*

Although the previously described pathway is considered the most important autophagic route, autophagosomes generation can occur also at the soma, in the mid-axon or at dendrites, where they move in a bidirectional-oscillatory manner (Maday and Holzbaur 2014; Maday and Holzbaur, 2016). An example is the degradation through lysosomes recruited at postsynaptic sites to guarantee a proper local regulation of synaptic machinery (Kulkarni and Maday, 2018b).

Autophagy is important in multiple aspects of synaptic physiology: it regulates synapse formation and pruning, synaptic proteostasis, it is required to maintain the pool of functional SVs, and it regulates the level of post-synaptic scaffolding proteins and NT receptors. Several evidence indicate an enhanced activity-dependent autophagic induction within presynaptic and postsynaptic terminals, identifying autophagy as a key regulator of synaptic plasticity and transmission in response to neuronal activity (Hernandez et al., 2012; Vijayan and Verstreken, 2017). Along this line, recent evidence demonstrated that autophagy induction is required for activity-dependent structural and functional plasticity underlying novel memory formation *in vivo* (Glatigny et al., 2019). Curiously, nutrient deprivation results ineffective in inducing autophagy in neurons, indicating that the role of autophagy in this type of cell primarily relies in the maintenance of homeostasis, rather than producing basic nutrients during starvation (Maday and Holzbaur, 2016).

Besides their conventional function as degradative organelles, a subset of autophagosomes appears to act as signaling organelles able to retrogradely transport BDNF-activated TrkB receptors internalized at the presynapse towards the soma, thus unveiling a novel non-degradative role of autophagosomes at presynaptic boutons (Kononenko et al., 2017; Andres-Alonso et al., 2019).

### 1.1.3 Synaptic vesicle endocytosis

As previously mentioned, a key point in neuronal activity is neurotransmission, a process triggered by a spike in intracellular calcium concentration at presynaptic level and consisting in the release of NT in the synaptic cleft through the fusion of SVs with the plasma membrane at the level of the active zone (AZ) of nerve terminal. This event occurs together with compensatory local membrane retrieval by endocytosis, in order to maintain the availability of SVs of proper size and composition, and to prevent an abnormal extension of the presynaptic membrane with a consequential loss of

membrane tension and alterations in presynaptic structure location (Kononenko and Haucke, 2015; Soykan et al., 2016).

Currently there are four proposed models of SV recycling that differs for their speed, dependence on clathrin and its associated factors, and cargo fidelity: kiss and run endocytosis, clathrin-mediated endocytosis, ultrafast endocytosis and activity dependent bulk endocytosis (**Fig. 6**). It is possible that the dominant mode for presynaptic membrane retrieval and SV reformation depends on the type of neuron and its activity pattern.

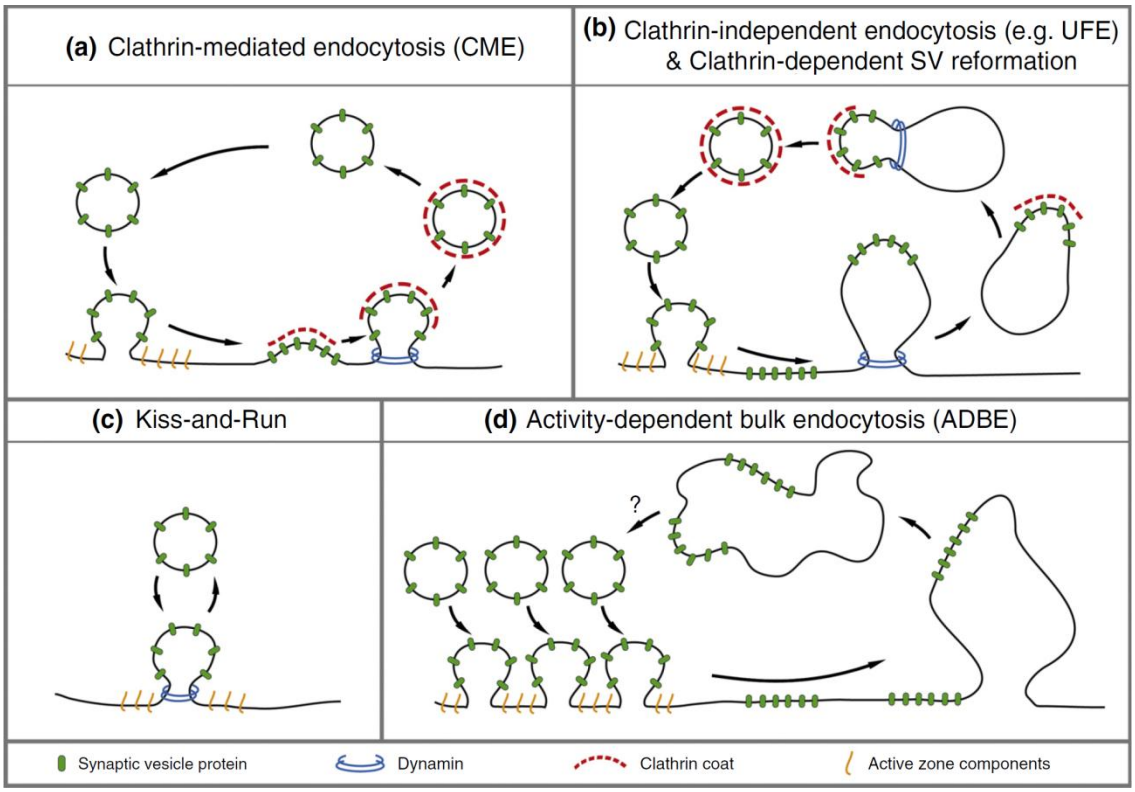


**Figure 6: Schematic overview of proposed SV recycling models.**

(a) In CME SVs fully fuse with the AZ membrane and are recycled through the assembly of a clathrin coat that mediates the membrane invagination, followed by the release of CCVs to reform SVs post-uncoating. (b) In UFE SVs rapidly fully fuse with the AZ membrane and large cisternal structures are retrieved in the synapse, by which new SVs are generated through CME. (c) SVs transiently fuse with the AZ membrane without collapsing, and immediatly close. (d) Multiple SVs simultaneously fuse with the AZ membrane, followed by bulk membrane retrieval at distal sites, by which SVs are reformed both involving or not clathrin. *Image reprinted from Current Opinion in Neurobiology, Vol. 39, T. Soykan, T. Maritzen, V. Haucke, Modes and mechanisms of synaptic vesicle recycling, Pages 17-23, Copyright 2016, with permission from Elsevier.*

**Kiss and run endocytosis** – A fast (≤ 1 s) membrane retrieval model is represented by kiss and run that occurs directly at the AZ (Ceccarelli et al., 1972). It consists in the transient fusion SVs without collapse of the vesicle, and involves the formation of a transient pore for NT release, that immediatly closes manteining inalterated the original molecular composition of the vesicle (Kononenko and Haucke, 2015; Soykan et al., 2016).

**Clathrin-mediated endocytosis (CME)** – CME is the most studied and best characterized endocytic model in eukaryotic cells (McMahon and Boucrot, 2011). It consists in a slow (10-20 s) SV recycling mechanism that differs from the previously described pathways for its dependence by clathrin, in form of a big complex called triskelion composed of three clathrin heavy chains interacting with three clathrin light chains (Kirchhausen et al., 2014), and the assembly protein complex 2 (AP-2), a big multimeric complex composed of two subunits, called ears, and a big core complex, in turn composed of two large α and β2 subunits, a medium-sized μ subunit and a small δ2 subunit (**Fig. 7**) (Collins et al., 2002). In CME vesicles, after a complete fusion with the plasma membrane, are retrieved through the formation of clathrin-coated vesicles (CCVs), which, following uncoating, reenter the SVs pool. Invaginations start with the assembly of a clathrin coat formed by clathrin triskelia, initiated by early acting endocytic adaptors such as AP-2, that mediates transmembrane cargo selection and coordinates the coat-assembly (Beacham et al., 2019). AP-2 is found in the cytosol in its “close” inactive state, but in response to phosphatidylinositol-4,5-bisphosphate (PI2P) conjugation its conformation changes to an “open” active state, that allows its association to the AZ membrane through its core, and the interaction of ears subunits with the clathrin coat (**Fig. 7**). The process starts with the formation of early shallow clathrin-coated pits (CCPs), that undergo to maturation during which they progressively invaginate, and finally the GTPase dynamin catalyzes membrane scission and release of CCVs. CCPs are observed on the presynaptic membrane, often lateral to AZs, but also on internal endocytic cisternae, some of which may be connected with the plasma membrane (Takei et al., 1996; Ferguson et al, 2007; Kononenko et al., 2014; Watanabe et al., 2014; Camblor-Perujo and Kononenko, 2021).

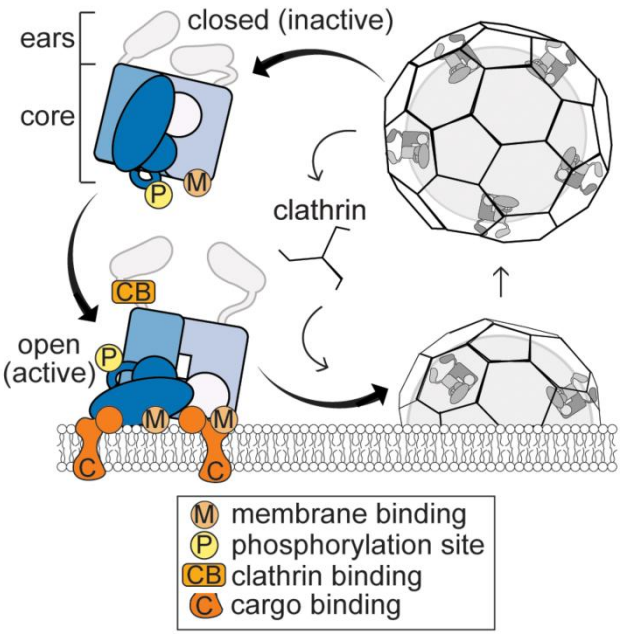


**Figure 7: Structure and function of AP-2**
The assembly protein complex 2 (AP-2) is big multimeric complex composed by a big core complex that mediates AP-2 membrane association and cargo binding, and by two subunits called ears, that bind clathrin triskelia. In its close conformation, the membrane and clathrin binding is repressed and AP-2 is in inactive state, while in its open conformation AP-2 is in its active state and the binding with membranes and clathrin is promoted, allowing the formation of clathrin coated vesicles. *Image modified from Beacham et al., 2019.*

**Ultrafast endocytosis (UFE)** – Synapses, in addition to CME, capitalize on clathrin-independent mechanisms of membrane retrieval, such as ultrafast endocytosis (UFE) and bulk endocytosis. UFE owes its name to its extreme rapidity (50-500 ms) and occurs by complete fusion of SVs to the AZ of the plasma membrane followed by the retrieval of large cisternal structures that form laterally to the AZs. New SVs are regenerated from these structures through a slow, presumabily clathrin-dependent mechanism (Watanabe et al., 2013a, 2013b, 2014).

**Activity-dependent bulk endocytosis (ADBE)** – ADBE is a slow (>1 s) non-selective mechanism consisting in the retrieval of large endocytic vacuoles from the plasma membrane, distal from the AZ, consequentially converted into SVs via clathrin-dependent and/or clathrin-independent mechanisms (Cheung and Cousin, 2013). This pathway is considered an emergency measure in response to prolonged high-frequency stimulation to prevent a block of neurotransmission (Kononenko and Haucke, 2015; Soykan et al., 2016).

### 1.1.4. Endocytosis and autophagy

Multiple aspects of neuronal physiology, the communication with the environment and the maintenance of protein and organelle homeostasis, crucially depend on endocytosis and autophagy. Interestingly, several proteins with a well-known function in the regulation of SV recycling have recently been reported to participate in the

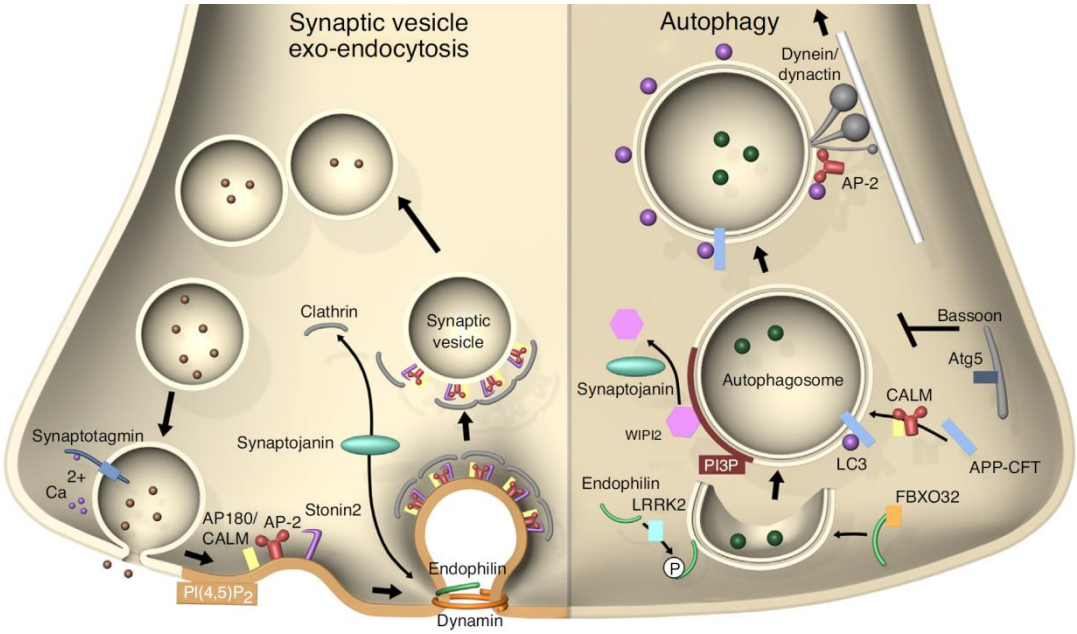


**Figure 8: Schematic overview of autophagy (right) and synaptic endocytosis (left) crosstalk.** *Image modified from Azarnia Tehran et al., 2018.*

endosome-autophagosome trafficking at presynaptic terminals (**Fig. 8**) (Azarnia Tehran et al., 2018; Overhoff et al., 2020). In fact, many evidence highlight a strong interconnection between these pathways in neurons, even if the reciprocal regulation of these systems is still matter of debate. This molecular crosstalk between SV recycling and autophagy may provide an activity-dependent quality control mechanism needed to guarantee an adequate NT release, and it is at the end crucial for proper brain function.

An efficient rejuvenation of SV proteins has been shown to facilitate neurotransmission in *Drosophila* (Fernandes et al., 2014; Uytterhoeven et al., 2011). Depletion of the presynaptic protein Atg5-interactor Basoon results in the increasing of autophagy and decreasing of SV density at presynaptic terminals (Okerlund et al., 2017). Hernandez and colleagues reported a strong interdependence between autophagy induction and the number of SVs in dopaminergic neurons (Hernandez et al. 2012). Moreover, two research groups demonstrate that endophilin-A, an endocytic dynamin interactor essential for SV recycling, is involved in autophagosome formation and its deletion interferes with autophagosomes generation (Murdoch et al., 2016; Soukup et al., 2016). Similarly, Rab7, associated to late endosomes, is required for autophagosome formation, as well as autophagic retrograde transport and fusion with lysosomes (Cheng et al., 2015; Yap et al., 2018). Another example is the transport of the brain-derived neurotrophic factor (BDNF) and TrkB receptor to the soma, that

occurs by retrograde axonal transport via amphisomes after the fusion between BDNF/TrkB containing endosomes with autophagosomes (Andres-Alonso et al. 2019). In a study conducted by Kononenko and colleagues, AP-2 was shown to be involved, beyond its canonical role in CME, also in autophagosome retrograde transport by binding both LC3 and the dynactin subunit p150$^{Glued}$. AP-2 silencing, in fact, links to retrograde transport impairment and accumulation of endosome-like vacuoles (ELVs) and autophagosomes at presynaptic terminals and along axons (**Fig. 9**) (Kononenko et al., 2017). AP-2 results therefore an essential actor in the autophagosome-mediated transport of BDNF/TrkB (**Fig. 9**), thus promoting neuronal complexity and preventing neurodegeneration both *in vitro* and *in vivo* (Kononenko et al., 2017).

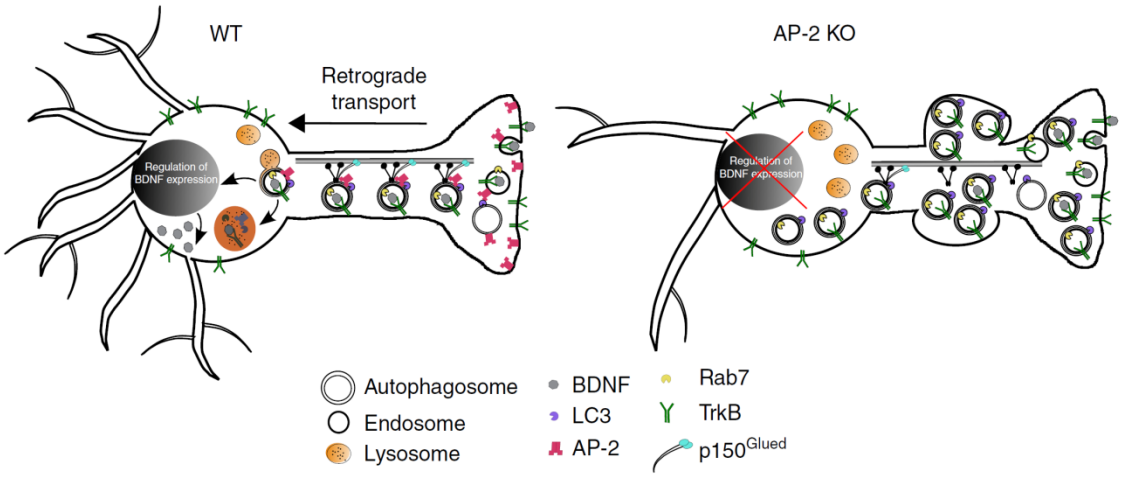


**Figure 9: Representation of autophagic dysfunctions in AP-2 KO neurons.**

"Hypothetical model for the role of AP-2 in retrograde transport of TrkB-containing autophagosomes in neurons. In WT neurons, AP-2 via its association with LC3 and p150Glued mediates retrograde transport of BDNF/TrkB-containing amphisomes (late-stage autophagosomes post-fusion with Rab7-positive late endosomes) to the cell body, where TrkB signalling regulates transcription of activity-dependent genes in the nucleus. In the absence of AP-2 (KO) TrkB endocytosis proceeds, however BDNF/TrkB-mediated signalling is defective due to impaired retrograde transport of BDNF/TrkB-containing autophagosomes. Stalled late-stage autophagosomes in neurites of AP-2 KO neurons cause axonal swellings and underlie neurodegeneration." *Image and legend reprinted from Nature Communications, Vol. 8, N. Kononenko, G. A. Claen, M. Kuijpers, D. Puchkov, T. Maritzen, A. Tempes, A. R. Malik, A. Skalecka, S. Bera, J. Jaworski, V. Haucke, Retrograde transport of TrkB-containing autophagosomes via the adaptor AP-2 mediates neuronal complexity and prevents neurodegeneration, Article 14819, Copyright 2017, open access article distributed by Springer under the terms of the Creative Commons Attribution 4.0 International License.*

### 1.1.5 Autophagy and Alzheimer Disease

Because of their extended lifespan and complex morphology, neurons are extremely susceptible to protein damage (Rubinsztein et al., 2011) and a proper function of autophagy is required for maintenance of synaptic homeostasis and neurotransmission (Maday, 2016; Kulkarni and Maday, 2018). Strong connections between the presynaptic machinery for SV exocytosis/endocytosis, autophagy and neurological disorders are emerging (Menzies et al., 2015; Wang et al., 2013). Defects in endocytosis and alterations in any stage of the autophagic pathway indeed link to various neurodegenerative diseases, such as Alzheimer Disease (AD), Parkinson Disease, Huntington Disease and Amyotrophic Lateral Sclerosis, as they directly impact on neuronal survival, synaptic transmission and plasticity (Nixon et al., 2013; Frake et al., 2015; Menzies et al., 2015; Azarnia Tehran, 2018; Bingol, 2018; Fujikake et al., 2018; Overhoff et al., 2020).

Since AD is considered the most prominent neurodegenerative disease and the primary cause of cognitive impairment during aging (Long and Holtzmann, 2019), in the last years a particular attention was focused on the link between this disease and autophagic dysfunctions. Functional alterations of the endosomal and autophagic pathways were indeed found to occur as early pathogenic events in AD neurons (Yao, 2004; Cao et al., 2010; Tamminemi et al., 2017), often preceding the neurotoxic insults, and directly contributing to abnormal amyloid production, synaptic dysfunction and reduced neuronal survival. AD is indeed characterized by an abnormal and neurotoxic accumulation at brain level of β-amyloid (Aβ) plaques, which are generated through the cleavage of the amyloid precursor protein (APP), and neurofibrillary tangles (NFTs), mainly composed by hyperphosphorilated Tau. An altered autophagic pathway may be a contributing factor for the deposition of these structures by both reducing their removal and promoting their production (Nilsson et al., 2013; Feng et al., 2017).

Experimental evidence raised in mouse models of AD and human AD indicates that, in addition to the extracellular accumulation of Aβ, its intracellular accumulation is also a very early event that even precedes the formation of amyloid plaques and correlates with early synaptic dysfunction (Gouras et al., 2000; Takahashi et al., 2002; Yang et al., 2015). This is accompanied by an expansion of the endosomal compartment and by a massive accumulation of unprocessed autophagic vacuoles that appear unable to properly mature upon fusion with late endosomes/lysosomes (**Fig. 10**) (Boland et al., 2008; Nixon and Yang, 2011) and positive for APP and APP-processing factors (Yu et al., 2005; Nilsson et al., 2013; Whyte et al., 2017). Moreover, a blockade of the

autophagic flux correlates with the accumulation of phosphorilated Tau (Lee et al., 2010; Rodríguez-Martín et al., 2013) while induction of autophagy contributes to decreasing of Tau levels and NFTs deposition (Berger et al., 2006; Krüger et al., 2012). This phenotype, distinctive for AD neurons, may be caused by an impairment in autophagosome retrograde transport, in their altered maturation or in a defective lysosomal clearance (Nixon et al.,2005; Boland et al., 2008; Lee et al., 2010; Rodriguez-Martin et al., 2013; Tamminemi et al., 2017). For instance, AP-2, previously mentioned for its double role in both SV recycling and autophagy, was reported to promote the intracellular trafficking and lysosomal degradation of BACE1, a β-secretase involved in APP processing, (Feng et al., 2017; Ye et al., 2017; Bera et al., 2020), and to target endosomal internalized APP for autophagic turnover, preventing amyloidosis (Tian et al., 2013). These findings suggest that AP-2 may be an important player in AD.

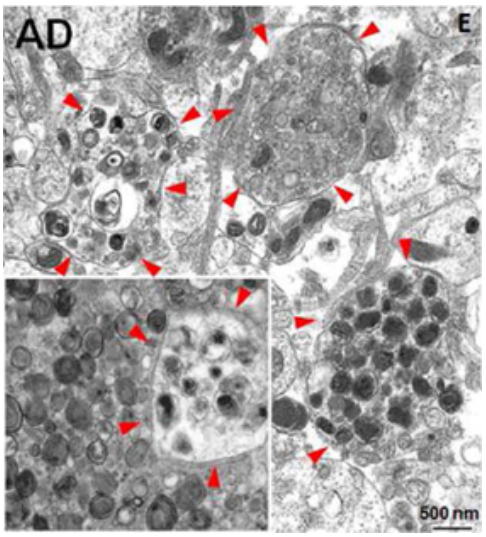


**Figure 10: Ultrastructural analysis of dystrophic AD neurites.**
AD neurons are affected by autophagic alterations that cause the severe accumulation of AVs (circled by arrowheads). *Image reprinted from Neurobiology of Disease, Vol. 43, Issue 1, R.A. Nixon and D.S. Yang, Autophagy failure in Alzheimer's disease—locating the primary defect, Pages 38-45, Copyright 2011, with permission from Elsevier.*

The increasing evidence of autophagic contribute to AD provide promising perspectives for development of new therapeutic approaches. Several studies indeed demonstrate that autophagy boosting with various autophagic activators on AD mouse model results in beneficial effects by limiting Aβ production and/or deposition and cognitive impairment (Spilman et al., 2010; Du et al., 2013; Zhu et al., 2013; Jiang et al., 2014). However, effects of autophagy upregulation in patients affected by AD have not been explored yet, furthermore the molecular mechanisms of therapeutic targeting of autophagy needs to be clarified.

## 1.2 APache (KIAA1107)

*KIAA1107* is an uncharacterized, highly evolutionary conserved gene. The research group supervised by prof. Silvia Giovedì and prof. Fabio Benfenati published a paper describing the functional role of this gene product, the protein KIAA1107, that they named APache (Piccini et al., 2017).

Using the bioinformatics approach GAMMA (GlobAl Microarray Meta-Analysis) (Wren JD, 2009) to search for uncharacterized genes associated with SVs and synaptic physiology, they identified *KIAA1107* with the highest score. KIAA1107 is an evolutionarily conserved protein with unknown structure and function. The murine *KIAA1107* gene is located on chromosome 5 and includes two splicing variants, one coding for a protein of 1,088 aa that is considered the main isoform (~140 kDa). The human *KIAA1107* gene is located on chromosome 1 and gives rise to one transcript. They cloned the main mouse isoform and discovered that it is a neuron-specific protein highly expressed in the cortex, hippocampus and striatum (**Fig. 11A,B**), developmentally regulated in both mouse brain and primary cortical neurons (**Fig. 11C,D**), and present in axons and at presynaptic terminals (**Fig. 11E,F**).

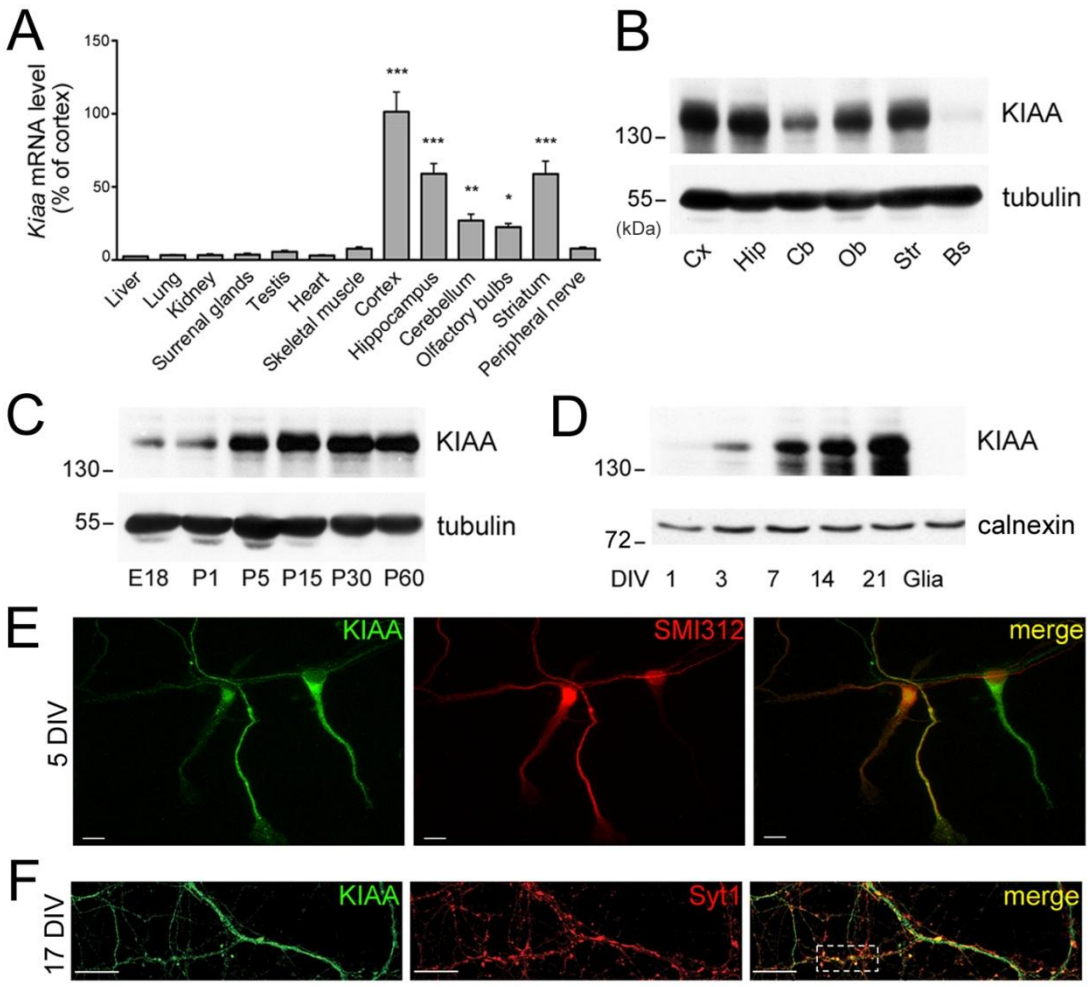


**Figure 11: Neuronal expression and localization of KIAA1107**

**(A)** Real-time PCR analysis of *KIAA1107* mRNA levels in various mouse tissues (means ± SEM, n=3 animals) *p<0.05, **p<0.01, ***p<0.001 vs liver, one-way ANOVA/Bonferroni's multiple comparison test. **(B)** Immunoblot of the regional expression of KIAA1107 in the adult mouse brain. Cx, cortex; Hip, hippocampus; Cb, cerebellum; Ob, olfactory bulb; Str, striatum; Bs, brain stem. **(C,D)** Immunoblot of the temporal expression profile of KIAA1107 in the developing mouse cerebral cortex **(C)** and in primary cortical neurons at various stages of development **(D)**. **(E,F)** Representative images of cortical neurons stained for KIAA1107 (green) and the pan-axonal neurofilament marker SMI312 (red) at 5 days in vitro (DIV) **(E)** or the presynaptic marker synaptotagmin-1 (Syt1, red) at 17 DIV (**F**). Scale bars, 10 µm. *Image and legend reprinted with permission from authors.*

They employed a mass spectrometry approach using overexpressed FLAG-KIAA1107 as a bait to pull-down KIAA1107 interactors from mouse brain extracts, and seven proteins were reproducibly identified as specific KIAA1107 binding partners (**Fig. 12A**). Interestingly, most of them (in red) are related to endosomal and autophagic trafficking. They focused the attention on AP-2, confirmed by co-immunoprecipitation assays the reciprocity of the interaction between KIAA1107 and AP-2 (**Fig. 12B**), and found the protein enriched on CCVs (**Fig. 12C**). In cortical neurons KIAA1107 immunoreactivity colocalized with AP-2 (**Fig. 12D**). Moreover, KIAA1107 silencing in mature neurons caused a reduction in the levels of AP-2 and of the SV protein synaptophysin compared to controls (**Fig. 12E**).

A

| Protein name | Gene name |
|---|---|
| Numb-like protein | NUMBL |
| Bcl-2 associated transcription factor 1 | BCLAF1 |
| V-type proton ATPase calatytic subunit A | ATP6V1A |
| Dynactin subunit 1 | DCTN1 |
| AP-2 complex subunit alpha-1 | AP2A1 |
| AP-2 complex subunit beta | AP2B1 |
| AP-3 complex subunit delta-1 (Human) / AP-3 complex subunit beta-2 (Mus Musculus) | AP3D1 / AP3B2 |

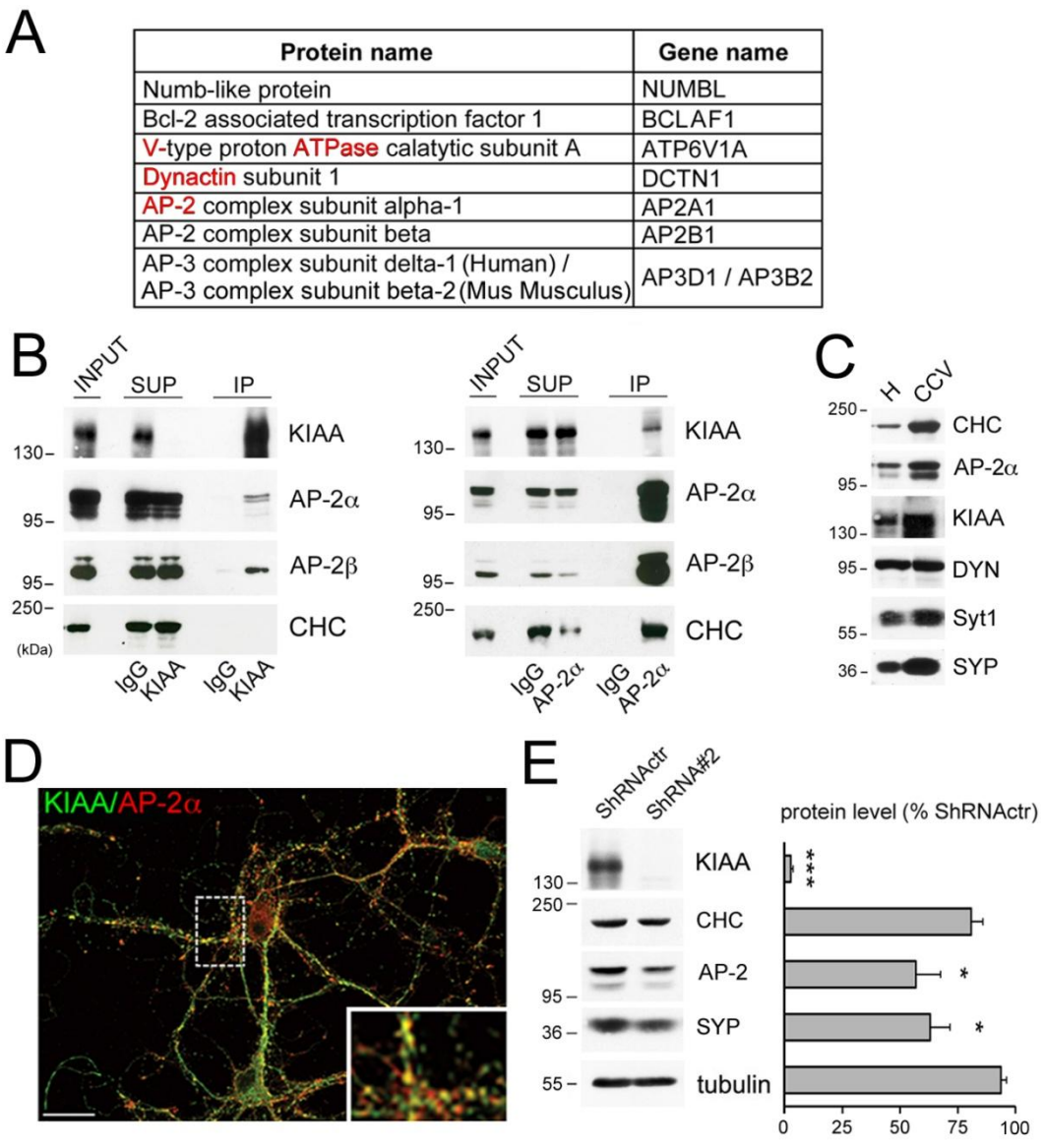


**Figure 12: KIAA1107 binds to AP-2 on clathrin-coated vesicles**

**(A)** KIAA1107 interactors identified by pull-down experiments and mass spectrometry analysis **(B)** Mouse brain extracts were subjected to immunoprecipitation (IP) with anti-KIAA1107 (left) or anti-AP-2α

antibodies (right) and control IgG (starting material, INPUT; supernatant, SUP). **(C)** KIAA1107 is enriched in the clathrin-coated vesicle (CCV) fraction (total homogenate, H; clathrin heavy chain, CHC; dynamin, DYN; synaptophysin, SYP). **(D)** Representative merged confocal image of cortical neurons (17 DIV) stained for KIAA1107 (green) and AP-2α (red). Scale bar, 10 µm. **(E)** Immunoblot and densitometric quantification of protein levels in silenced (ShRNA#2) and control neurons (means ± SEM, n=4 independent experiments). *p<0.05, ***p<0.001 vs ShRNActr, unpaired Student's t-test. *Image and legend reprinted with permission from authors.*

In light of this finding, KIAA1107 was named APache (AP2-interacting clathrin-endocytosis protein) and its characterization focused on its potential role in SV recycling. Experiments performed by silencing APache expression through RNA interference revealed that APache-lacking neurons were affected by a severe reduced SV and CCV density, accompanied by an accumulation of enlarged ELVs at presynaptic terminals, similarly to AP-2 knocked-down neurons, reflecting a function of APache in CME (**Fig. 13A,B**, additional evidence not shown). Moreover, APache downregulation *in vivo* leaded to an impaired maturation in developing neurons, that presented a reduction of total number and length of neurites, and significant defects in synaptic transmission in mature cultured neurons (data not shown). These experimental evidence indicate that APache is an important actor in the regulation of SV trafficking, neuronal development and synaptic plasticity.

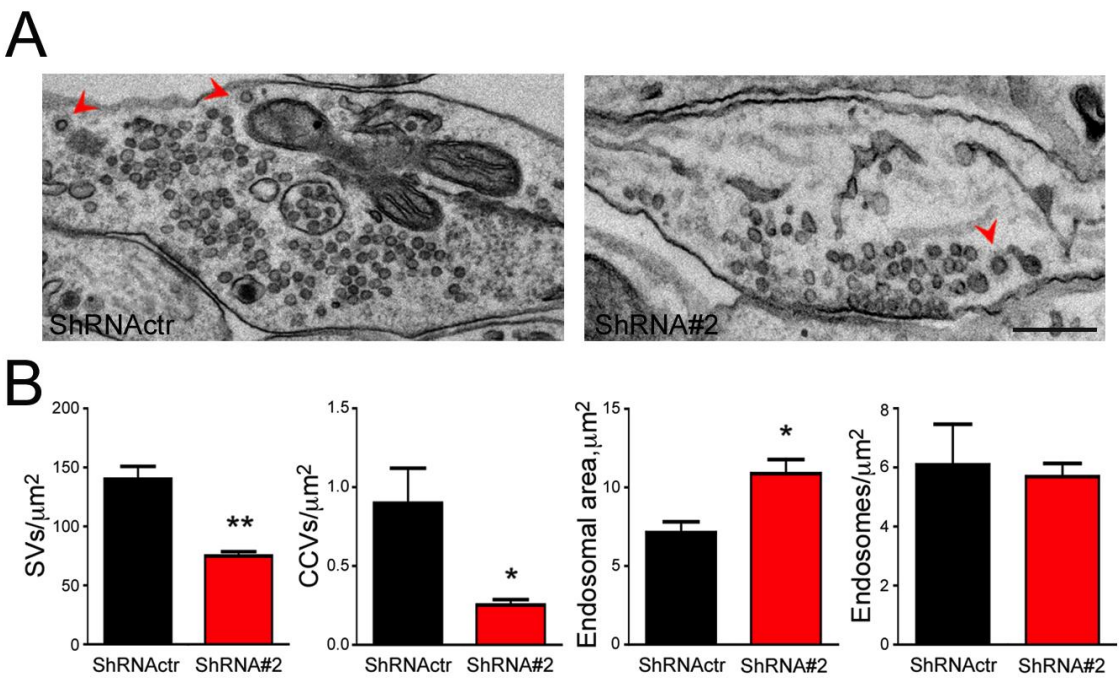


**Figure 13: Reduced SV density and increased size of endosome-like structures at APache-silenced cortical synapses**

**(A)** Representative TEM images of nerve terminals from cultured cortical neurons transduced with either ShRNActr or ShRNA#2 at 12 DIV and processed at 17 DIV. Note the reduced SV density in the APache-KD synapse compared to control (CCVs, red arrowheads). Scale bar, 200 nm. **(B)** Morphometric analysis from serial ultrathin sections obtained from ShRNActr (black bars) and ShRNA#2 (red bars) treated synapses revealed (from left to right) a reduction in the density of total SVs and CCVs and an increase in the area of endosome-like structures in APache-KD synapses compared to control. *p<0.05, **p<0.01, unpaired Student's t-test. *Image and legend reprinted with permission from authors.*

# 2. Aim of the study

The central hypothesis of this work was based on APache involvement in SV trafficking and association to AP-2, an important actor in neuronal endocytosis and autophagy, two processes that are severely affected in Alzheimer's disease (AD).

Our goal was the elucidation of APache functional role in neurons, especially in autophagy, to evaluate its potential contribution to the pathogenesis of the precocious neuronal defects observed in AD. This will help our understanding of the physiology of synaptic function, and at the same time, may open new avenues for translational research by assessing the impact of APache loss in specific processes of synapse functioning and of neuronal degeneration.

As experimental model we employed primary cultures of mouse cortical neurons, under autophagic stimulation or APache downregulation, and brain samples of late onset sporadic AD patients.

# 3. Materials and methods

## 3.1 Constructs

For APache silencing through lentiviral transduction 3 distinct short hairpin (sh) RNAs were designed (Mission shRNA custom cloning, Sigma-Aldrich) based on the sequence of the cloned KIAA1107 (APache) transcript variant (for detailed description of constructs see Piccini et al., 2017). ShRNA#2 resulted the most active in knocking down the endogenous APache expression and it was used for the subsequent studies. ShRNA#2 and control ShRNA (Luciferase shRNA; Sigma-Aldrich) were inserted into pLKO.1-CMV-mCherry lentiviral vectors. For rescue experiments, the p277-eGFP-APache vector was used, being intrinsically resistant to shRNA#2.

For APache silencing through transfection, ShRNA#2 and control ShRNA were inserted into pLKO.1-CMV-mTurquoise or pLKO.1-CMV-eGFP vectors. Autophagic flux was analyzed using the Tandem pBABE-puro mCherry-eGFP-LC3B plasmid (addgene, #22418). Autophagosome transport was analyzed using the pTagRFP-C-LC3B plasmid (Evrogen #FP141).

## 3.2 Cell culture and treatments

All the experiments were performed on mouse primary cortical cultures prepared from WT C57BL/6J (Charles River) 18-day embryos (E18). Cerebral cortices were washed in HBSS (Gibco #14175-053), dissociated by enzymatic digestion in 0.125% trypsin (Gibco #25050-14) for 25 min at 37°C and then triturated sequentially with a P1000 and a P200 pipette tip in Neurobasal (Gibco #21103-049) supplemented with 10% FBS (Gibco #10500-064), plus 1% Glutamax 100-X (Gibco #35050-38), 1% penicillin–streptomycin (Gibco #10378-016).

For imaging assays, neurons were plated at low density ($6x10^4$ cells/coverslip) onto 0.1 mg/ml poly-L-lysine (Sigma-Aldrich #25988-63-0)-coated 25-mm glass coverslips.

For biochemistry assays, neurons were plated at high density (300 × $10^6$ - 1 × $10^7$ cells/well) onto 1 mg/ml poly-L-lysine-coated 35-mm well plates. Neurons were maintained in Neurobasal supplemented with B27 (1:50 B27, Gibco #17504-007), 1% Glutamax, 1% penicillin–streptomycin at 37°C in a 5% $CO_2$ humidified atmosphere. Under this culture condition approximately 85-90% of the cortical neurons are glutamatergic and cultures are almost glia-free (Piccini et al., 2015).

Lentiviral transducion with pLKO.1-CMV-mCherry-ShRNA lentiviral vector was performed in neurons at 12 DIV (days in vitro) with 3 multiplicity of infection (MOI), and after 24 h medium was replaced with fresh and conditioned medium. Analysis was performed 5 days post infection (17 DIV). Control neurons were transducted with the corresponding control shRNA.

Transfection was performed in neurons at 10-14 DIV with Lipofectamine 2000 (Invitrogen #11668-19) according to the manufacturer's instructions, and cells were analysed after 72 h. Control neurons were transfected with the corresponding control shRNAs.

Torin1 treatment was performed by incubating neurons at 12-17 DIV with 250 nM Torin1 (BioVision #2273-5, resuspended in Milli-Q water) for 4 h at 37°C. Control neurons were incubated with sterile Milli-Q water (vehicle).

## 3.3 Biochemistry procedures

### 3.3.1 Protein extraction and subcellular fractionation

Total cell lysates were obtained from neurons at 12-17 DIV. Neurons were washed twice in ice-cold HBSS and lysed in lysis buffer (50 mM Tris; 150 mM NaCl; 1 mM EDTA pH 8.0; 1% Triton X-100) supplemented with protease and phosphatase inhibitor cocktail (Cell Signaling, respectively #58715 and #58705). After 10 min of incubation on ice, lysates were collected and clarified by centrifugation at 1,000 x g for 10 min at 4 °C to remove nuclei and unbroken cells.

For subcellular fractionation neurons at 12-17 DIV were washed twice in ice-cold HBSS and collected in buffered sucrose solution (0.32 mM Sucrose; 5 mM Hepes) supplemented with protease inhibitor cocktail. Cells were incubated on ice for 10 min and lysed by 10 passages through a 29G needle using a 1 ml syringe, then clarified by

centrifugation at 1,000 x g for 10 min at 4 °C to obtain post nuclear supernatant (PNS or S1 fraction). This was centrifuged at 16,000 x g for 15 min at 4 °C to obtain supernatant, a cytosolic fraction (S2) that was collected, and pellet, a membrane fraction (P2) that was resuspended in buffered sucrose solution.

Digitonin-based membrane-cytosol fractionation was performed on neurons at 12-17 DIV. Neurons were washed in ice-cold HBSS and permeabilized in buffer D (modified from Bernocco et al., 2008): 0.02% digitonin (Sigma-Aldrich #D-5628), 300 mM Sucrose, 5 mM Hepes, 100 mM NaCl, 5 mM EDTA, 3 mM $MgCl_2$ supplemented with protease inhibitor cocktail, under gentle shaking at 4°C for 20 min. Supernatant (cytosolic fraction) was collected, and membranes were scraped from the well plate in buffer D.

Protein lysates from autopsy sections of frontal cerebral cortex of late onset sporadic AD patients and cognitively normally aging elderly subjects were extracted in ice-cold buffered sucrose in homogenization buffer supplemented with protease inhibitor cocktail, and centrifuged at 1,000 x g for 10 min at 4 °C to obtain a PNS fraction.

### 3.3.2 Protein quantification and western blotting

Protein concentrations were determined using Bradford Protein Assay (Bio-Rad #5000006) or BCA Protein Assay kits (Thermo Scientific #23225) assays. Samples were boiled for 3 min in reducing sample buffer (Laemmli, 1970) and equivalent amounts of protein were subjected to SDS-PAGE electrophoresis on 10-14% polyacrylamide gels depending on target protein molecular weight, and transferred from the gel onto nitrocellulose membranes.

Blotted membranes were blocked for 1 h at room temperature in 5% milk in Tris-buffered saline (TBS: 200 mM NaCl, 50 mM Tris) plus 0.1% Triton X-100 (TBS-T) and incubated 2 h at room temperature or overnight at 4 °C with the following primary antibodies: anti-Actin (1:1000, Sigma #A4700), anti-Adaptin α (AP-2α) (1:1000, BD #610502), anti-Atg3 (1:1000, Cell Signalling #3415P), anti-Atg5 (1:1000, Cell Signalling #8540P), anti-ATP6V1A (1:5000, Abcam #ab137574), anti-Cathepsin D (1:2000, Sigma-Aldrich #219361), anti-KIAA1107 (1:1000, Primm EFA/10 201010-00019), anti-LAMP1 (1:1000, Abcam #ab24170), anti-LC3B (1:1000, Sigma-Aldrich #L7543), anti-mTOR (1:1000, Cell Signaling #2983), anti-phospho-mTOR(Ser2448) (1:1000, Cell Signaling #5536), anti-NaK3 (ATP1A3) (1:1000, Invitrogen #MA3-915), anti-Synaptophysin 1 (p38) (1:5000, SYSY #101 011), anti-Rab5 (1:1000, Abcam #

ab18211), anti-Rab7 (1:1000, Abcam ab50533), anti-Synapsin I (clone 10.22) (1:1000, homemade by Greengard's laboratory; Rockefeller University, NY, USA), anti-Synaptotagmin 1 (1:1000, SYSY #105 011), anti-Vinculin (1:5000, Sigma-Aldrich #V9264).

Membranes were washed in TBS-T and incubated for 1 h at room temperature with horseradish peroxidase (HRP)-conjugated goat anti-rabbit (1:3000; Bio-Rad #170-6515) or anti-mouse (1:5000; Bio-Rad #170-6516) secondary antibodies. Membranes were then washed in TBS-T and TBS. Bands were revealed with the ECL chemiluminescence detection system (Thermo Scientific #32106) with the ChemiDoc imaging system (Bio-Rad Laboratories, Hercules, CA, USA) and the quantification of immunoreactivity was performed by bands densitometric analysis with ImageJ/FIJI (Rasband, W.S., ImageJ, U. S. National Institutes of Health, Bethesda, MD, USA).

### 3.3.3 Cathepsin D (CTSD) activity assay

CTSD activity was determined in 17 DIV neurons using a CTSD activity assay kit (BioVision #K143) as described by the manufacturer's protocol. Enzymatic activity was determined using a CTSD substrate (Gly-Lys-Pro-Ile-Leu-Phe-Phe-Arg-Leu-Lys(DNP)-D-Arg-NH2 trifluoroacetate salt) labeled with MCA that releases fluorescence after the substrate cleavage. Briefly, neurons were lysed in 200 µl of chilled CD Cell Lysis Buffer, incubated on ice for 10 min, and centrifuged for 5 min at top speed. Ten µg /well of cell lysate was mixed with 50 µl of Reaction Buffer and 2 µl of substrate to a final volume of 102 µl into a 96-well plate and incubated for 2 h at 37 °C. Samples were read at 10-min intervals (Ex/Em= 328/393 nm) with the multiplate TECAN® reader (Tecan Trading AG, Switzerland) using a 320 ± 25-nm excitation filter and 485 ± 20-nm emission filter. Background values were calculated by reading wells filled only with solutions and subtracted to each sample values. Data were normalized to µg protein/sample and expressed in percentage of control value.

## 3.4 Microscopy

### 3.4.1 Transmission electron microscopy (TEM)

Neurons were fixed at 17 DIV with 1.2% glutaraldehyde in 66 mM sodium cacodylate buffer, post-fixed in 1% $OsO_4$, 1.5% $K_4Fe(CN)_6$, 0.1 M sodium cacodylate, en bloc stained with 10% of uranyl acetate replacement stain (EMS) for 30 min, dehydrated, and flat embedded in epoxy resin (Epon 812, TAAB). After baking for 48 h, the glass coverslip was removed from the Epon block by thermal shock and neurons were identified by means of a stereomicroscope. Embedded neurons were then excised from the block and mounted on a cured Epon block for sectioning using an EM UC6 ultramicrotome (Leica Microsystems). Ultrathin sections (60–70 nm thick) were collected on 200-mesh copper grids (EMS) and observed with a JEM-1011 electron microscope (Jeol, Tokyo, Japan) operating at 100 kV. For each experimental condition, at least 50 images were acquired at 10,000x magnification (sampled area per experimental condition: 36 $\mu m^2$). Synaptic profile area, AV number and density were determined using ImageJ/FIJI. AVs were defined as single or double membrane-bound vacuoles containing intracellular material.

### 3.4.2 Immunocytochemistry and confocal microscopy

Neurons at 12-17 DIV were washed in pre-warmed phosphate-buffered saline buffer (PBS) and fixed with pre-warmed 4% paraformaldehyde (PFA; Thermo Scientific #28908) plus 4% sucrose for 15 min at room temperature. Fixation process was followed by serial washes in PBS.

All the following steps were performed at room temperature. Cells were permeabilized in 0.1% PBS with 0.1% Triton X-100 (PBS-T) for 10 min, followed by blocking in PBS-T with 3% bovine serum (BSA, Sigma-Aldrich #A4503) for 30 min. Neurons were incubated for 2 h (or overnight, at 4 °C) with the following primary antibodies: anti-KIAA1107 (1:500, Primm EFA/10 201010-00019), anti-LAMP1 (1:200, Sigma #L1418), LC3B (N-term) (Clone 2G6) (1:100, Origene #AM20213PU-N), LC3B (1:200, Sigma #L7543), p62/SQSTM1 (1:500, Sigma #P0067), Rab7 (1:250, Abcam #ab137029), Synaptobrevin 2 (VAMP2) (1:500, SYSY #104 211).

Cells were then washed in PBS and labeled with the following fluorochrome-conjugated antibodies (Invitrogen; all 1:500): Alexa Fluor goat anti-mouse 488 (#A11001), Alexa Fluor goat anti-rabbit 488 (#A11034); Alexa Fluor goat anti-mouse 647 (#A21235), Alexa Fluor goat anti-rabbit 647 (#A21244). Incubation was followed by serial washes in PBS-T and PBS. 25 mm coverslips were mounted using Prolong Gold

antifade reagent with or without DAPI (4′, 6′-diamidino-2- phenylindole) for nuclear staining (Thermo Scientific, respectively #P36934 and #P36935).

Images of neurons were acquired with a confocal laser scanning microscopy (CLSM; Leica SP8, Leica Microsystems, Wetzlar, Germany) using a 40 × oil-immersion objective. Acquisitions consisted of stacks of images taken through the z-plane of the cell. Confocal microscope settings were kept the same for all scans in each experiment. Image analysis of different stacks in each colour channel was performed using the JACoP plug-in on ImageJ/FIJI for colocalization studies with Manders test. For quantitative analysis of fluorescent VAMP2-puncta, masks of mCherry-infected neurons were made using ImageJ. Then VAMP2 signal was thresholded using the same parameters for all the images. Colocalization points represent VAMP2 puncta of only infected neurons and their number was determined using the ImageJ/FIJI colocalization plugin. The VAMP2 puncta density was calculated as the number of puncta on the infected neuronal area.

### 3.4.3 Live-cell imaging

Images from neurons at 13 DIV were acquired in Tyrode's solution (10 mM glucose, 140 mM NaCl, 2.4 mM KCl, 10 mM Hepes, 2 mM $CaCl_2$, 1 mM $MgCl_2$) at temperature-controlled stage (37°C) with an inverted epifluorescence microscope (Olympus IX81, Olympus Corporation, Tokyo, Japan) using a 60 × oil-immersion objective. Axons are identified by their morphology and autophagosomes were tracked within axonal tracts around 25 µm of length. Time-lapse images were acquired for 30 sec (1Hz) with xCellence rt (Olympus). Kymograph construction was carried out using the KymographBuilder plug-in in ImageJ/FIJI. Particles were manually tracked with the Manual Tracking plug-in on ImageJ/FIJI.

## 3.5 Statistical analysis

Data distribution was assessed by D'Agostino-Pearson's normality test (n>6) or Shapiro-Wilk test (n≤6). The comparison between two normally distributed sample groups was performed using the unpaired Student's two-tailed *t*-test with Welch's correction, while two groups not normally distributed were compared using the nonparametric Mann-Whitney's *U*-test. To compare more than two experimental groups, either the one-way or two-way ANOVA (followed by the Bonferroni's multiple

comparison test) or the Kruskal-Wallis ANOVA (followed by the Dunn's multiple comparison test) was used depending on data distribution. Statistical analysis was performed with GraphPad Prism version 7.00 (GraphPad Software, Inc., San Diego, CA, USA). Significance level was set to $p<0.05$. Experimental data are expressed as means ± SEM for number of cells/samples or independent preparations (n) as reported in the figure legends.

# 4. Results

## 7.1 APache is induced by autophagy stimulation and colocalizes with LC3 on autophagosomes

As first step we wanted to assess if APache is involved in autophagy by promoting the process in mouse primary cultured cortical neurons at 12-17 DIV with the inducer molecule Torin1 (250 nM, 4 h), that act as an mTOR inhibitor, and analyzed the samples through western blot assay. First, to confirm the efficacy of Torin1 treatment, we measured the expression level of the autophagic marker LC II, the active form of LC3 bound to autophagosome membranes, that resulted higher in treated neurons compared to control (vehicle) cells (**Fig. 14A,B**), confirming the actual induction of the autophagic cycle. We proceed by measuring the expression level of APache: in Torin1 treated neurons the expression level of APache was significantly increased compared to control neurons (**Fig. 14A,B**). Moreover, also the level of the α subunit of the APache interactor AP-2 (AP-2α) resulted significantly augmented in treated neurons, compared to control samples (**Fig. 14A,B**).

To confirm the increased APache level after autophagy stimulation, we then analyzed Torin1 treated and control neurons through immunocytochemistry assay. Torin1 efficacy was verified by measuring the fluorescence intensity of LC3: as expected, LC3 signal increased consequentially to the treatment (**Fig. 14C,D**). APache fluorescence intensity in treated neurons also resulted significantly higher compared to control cells signal (**Fig. 14C,E**). Furthermore, compared to controls, treated neurons showed a higher colocalization between LC3 and APache signals (**Fig. 14F**). These results suggest that autophagy stimulation in neurons with Torin1 promotes APache induction and colocalization with LC3 on autophagosomes.

In neurons, autophagosomes mainly form at synaptic level (Maday and Holzbaur, 2016; Kulkarni and Maday, 2018a). To evaluate the synaptic response to autophagy induction, we checked for autophagosome presence at synaptic level in control and Torin1 treated neurons through immunocytochemistry assay. We measured the

fluorescence intensity of LC3 at level of puncta positive for the synaptic marker VAMP2, and treated cells showed a significantly higher signal compared to controls **(Fig. 14G,H)**, confirming the increased formation of autophagosomes at synaptic level after autophagy induction. We then passed to the evaluation of APache reaction to autophagic induction at synaptic level, and we measured the signal of APache in VAMP2 positive-puncta. Similarly to LC3, APache fluorescence intensity resulted significantly increased in treated neurons compared to control cells **(Fig. 14I,L)**, indicating that APache increasing observed in neurons occurs also at synapses.

In order to probe if APache may therefore be directly involved in autophagy pathway, we first wanted to better analyze its localization within neurons by performing different methods of subcellular fractionation of cultured cortical neurons at 12-17 DIV. We first performed a cytosolic- (S2) and membrane-enriched (P2) fractionation, analyzed through western blot. APache, besides been present at detectable level in cytosolic fraction, resulted significantly enriched in membrane fraction, validated by the concomitant increased level of synapsin I (Syn I) and synaptophysin (p38), two SV membrane markers, in P2 fraction (**Fig. 15A,B)**. Then, we performed a subcellular fractionation with the detergent digitonin to extract cytosolic soluble proteins (cytosol fraction) from plasma membrane and organellar proteins (membrane fraction). Digitonin indeed partially solubilizes only the plasma membrane, and not all cellular membranes (Bernocco et al., 2008). The efficiency of the protocol in generation of extracts corresponding to different subcellular structures was validated by western blot analysis with antibodies specific for protein markers: vinculin as cytosolic marker, $Na^+/K^+$ ATPase as plasma membrane marker, LC3 II and LAMP1 as autophagic markers. LC3 II and LAMP1 were almost exclusively found in membrane fractions compared to cytosolic ones, verifying an efficient purification of autophagosomes and autolysosomes (**Fig. 15C,D**). APache distribution showed an appreciable enrichment in the membrane fraction compared to cytosol (**Fig. 15C,D**), confirming the presence of the protein at autophagic vacuolar level.

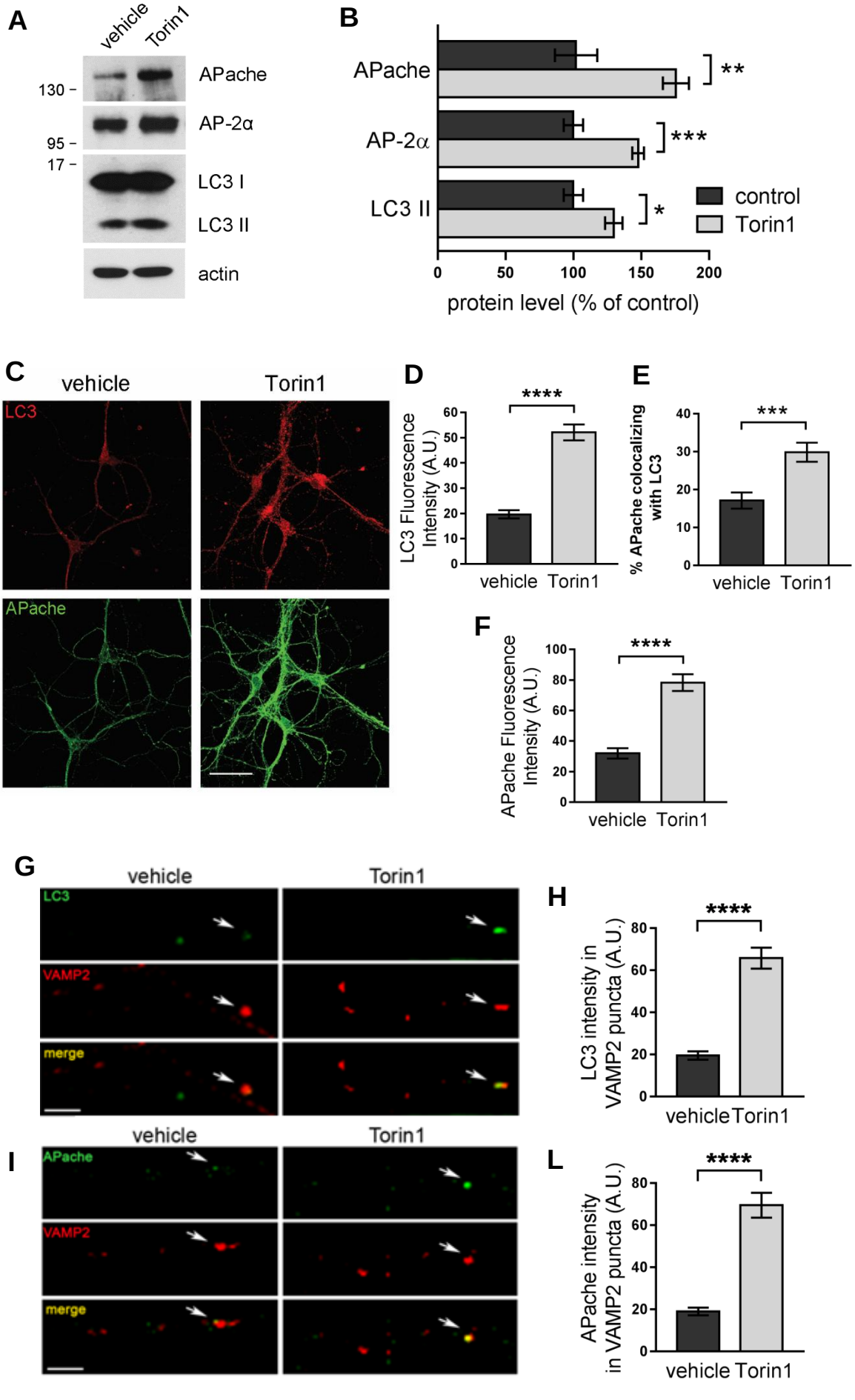
A
vehicle
Torin1
130 –
95 –
17 –
APache
AP-2α
LC3 I
LC3 II
actin
B
APache
AP-2α
LC3 II
**
***
*
control
Torin1
0
50
100
150
200
protein level (% of control)
C
vehicle
Torin1
LC3
APache
D
LC3 Fluorescence Intensity (A.U.)
****
vehicle
Torin1
E
% APache colocalizing with LC3
***
vehicle
Torin1
F
APache Fluorescence Intensity (A.U.)
****
vehicle
Torin1
G
vehicle
Torin1
LC3
VAMP2
merge
H
LC3 intensity in VAMP2 puncta (A.U.)
****
vehicle
Torin1
I
vehicle
Torin1
APache
VAMP2
merge
L
APache intensity in VAMP2 puncta (A.U.)
****
vehicle
Torin1

**Figure 14: Increased APache protein levels after autophagy stimulation.**

**(A)** Representative western blotting of lysates from cultured cortical neurons treated with either DMSO (vehicle) or the mTOR inhibitor Torin1 (250 nM, 4h) at 17 DIV; immunoreaction performed with antibodies against APache, AP-2α and LC3 II (lower band) and actin, used as loading control. **(B)** Quantification of APache level (vehicle: 100 ± 15.28; Torin1: 172.2 ± 8.38, n=6 independent preparations), AP-2α level (vehicle: 100 ± 7.18; Torin1: 147.7 ± 4.3, n=6 independent preparations) and LC3 II level (vehicle: 100 ± 7.13; Torin1: 129.8 ± 6.39; n=6 independent preparations). Protein levels in treated neurons are expressed in percentage of the respective amounts in control neurons. Values are normalized on loading control. **p<0.01, ***p<0.001, Unpaired t test with Welch's correction. Graph shows means ± SEM. **(C)** Representative confocal images of cortical neurons treated with either vehicle or Torin1 (250 nM, 4 h) at 17 DIV and stained for LC3 (red) and APache (green). Scale bar, 20 µm. **(D, E)** Quantification of LC3 intensity values **(D)** (vehicle: 19.68 ± 1.60; Torin1: 52.13 ± 3.15, n=36-44 neurons per condition from n=3 independent preparations), APache intensity values **(E)** (vehicle: 31.96 ± 3.40, n=35 neurons; Torin1: 78.31 ± 5.53, n=40 neurons from 3 independent preparations) and percentage of APache and LC3 co-localization **(F)** (vehicle: 17.10 ± 2.13, n=26 neurons; Torin1: 29.85 ± 2.50, n=22 neurons from 3 independent preparations) in vehicle and Torin1 treated neurons. A.U. = arbitrary units of fluorescence intensity. ***p<0.001, ****p<0.0001, Unpaired t test with Welch's correction/ Mann-Whitney Unpaired t test. All graphs show means ± SEM. **(G,I)** Representative images of synapses from cortical neurons treated with either vehicle or Torin1 and stained for VAMP2 (red), to identify synaptic boutons, and either LC3 (green, **G**) or APache (green, **I**) at 17 DIV. Arrows denote synaptic boutons positive for LC3 or APache. Scale bar, 5 µm. **(H,L)** Quantification of LC3 **(H)** or APache **(L)** intensity values at VAMP2-positive puncta in vehicle and Torin1 treated synapses (LC3 vehicle: 19.50 ± 1.95, n=88 synapses; LC3 Torin1: 65.78 ± 4.99, n=89 synapses; APache vehicle: 18.99 ± 1.18, n=87 synapses; APache Torin1: 69.56 ± 5.94, n=82 synapses, from 3 independent preparations). A.U. = arbitrary units of fluorescence intensity. ****p<0.0001, Mann-Whitney Unpaired t test. All graphs show means ± SEM.

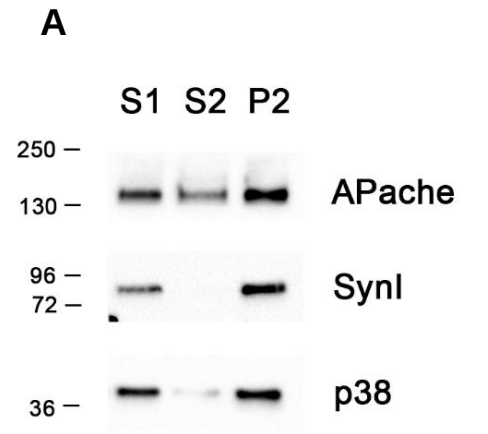
A
S1 S2 P2
250
130
96
72
36
APache
SynI
p38

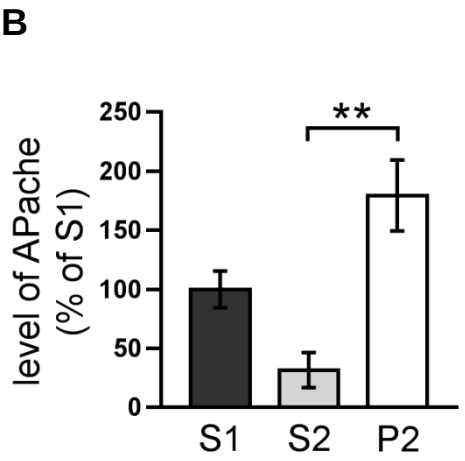
B
level of APache
(% of S1)
250
200
150
100
50
0
**
S1
S2
P2

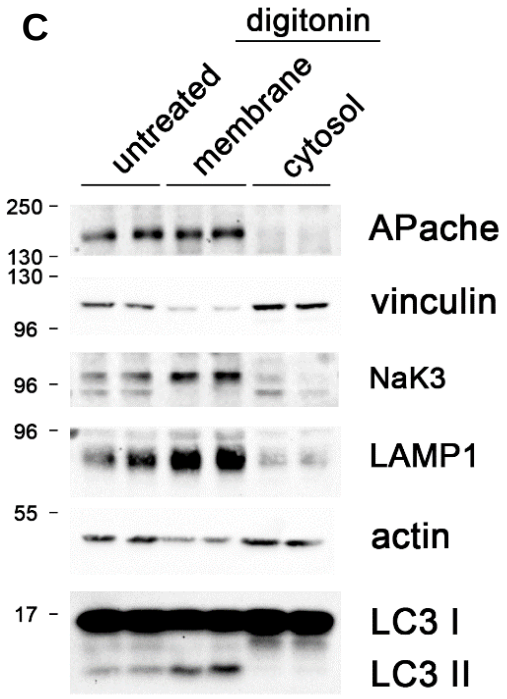
C
digitonin
untreated
membrane
cytosol
250
130
130
96
96
96
55
17
APache
vinculin
NaK3
LAMP1
actin
LC3 I
LC3 II

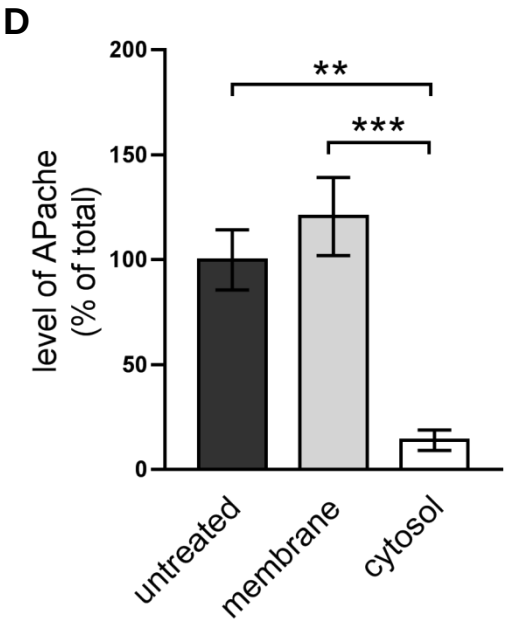
D
level of APache
(% of total)
200
150
100
50
0
**
***
untreated
membrane
cytosol

**Figure 15: APache is present at the level of autophagic vacuolar fraction**

(**A)** Representative western blotting of post nuclear supernatant (S1), cytosolic- (S2) and membrane-enriched (P2) fractions from cultured cortical neurons at 12-17 DIV; immunoreaction performed with antibodies against APache, synapsin I (Syn I) and synaptophysin (p38). Syn I and p38 are used as SV membrane markers. **(B)** Quantification of APache level (S1: 100 ± 15.67; S2: 31.57 ± 14.79; P2: 179.5 ± 30.17; n=5 independent preparations) expressed in percentage of the respective amount in post nuclear supernatant. **p<0.01, Kruskal-Wallis test. Graph show means ± SEM. **(C)** Representative western blotting run in duplicate of total lysates (untreated), organellar/plasma membrane and cytosolic preparations from cultured cortical neurons at 12-17 DIV; immunoreaction performed with antibodies against APache, vinculin, $Na^+/K^+$ ATPase α-3 (NaK3), LAMP1, LC3 II and actin. LC3 II and LAMP1 are used as protein markers respectively of autophagosomes and lysosomes to confirm the enrichment of autophagic vacuolars (autophagosomes and autolysosomes) in membrane fractions. Vinculin is used to evaluate potential cytosolic contaminations in organellar fractions and used as cytosolic loading control. NaK3 is used as membrane loading control. Actin is used as untreated total loading control. **(D)** Quantification of APache distribution in each fraction expressed in percentage of the respective amount in untreated total samples (untreated: 100 ± 13.29; membrane: 132.8 ± 20.58; cytosol: 17.68 ± 5.86; n=6 independent preparations). Values are normalized on the respective loading controls. **p<0.01, ***p<0.001, Ordinary one-way ANOVA. All graphs show means ± SEM.

## 7.2 APache silencing causes an aberrant autophagic accumulation also at synaptic level

Our previous results made us wonder if lack of APche may influence the autophagic pathway. To investigate this point, we silenced APache expression in mouse cortical neurons at 12 DIV through lentiviral transduction with a silencing mCherry-shRNA (APache KD), using a control mCherry-RNA for control neurons (control). First, cells were analyzed at 17 DIV by transmission electron microscopy (TEM) both at synaptic and neuritic level to check for autophagosome presence (**Fig. 16A,D**). In neurons, indeed, autophagosomes mainly form at synaptic level (Maday and Holzbaur, 2016; Kulkarni and Maday, 2018a). The constitutive presence of autophagosomes is considered physiological in neurons, but is rather limited, and an increase in the number and/or density of autophagosomes can therefore correlate with autophagic dysfunctions (Nixon et al., 2013; Zhang et al., 2013; Frake et al., 2015; Menzies et al., 2015; Azarnia Tehran, 2018; Bingol, 2018; Fujikake et al., 2018; Mizushima and Murphy, 2020; Overhoff et al., 2020). Compared to controls, in APache KD neurons a higher percentage of synapses accumulated autophagic vacuoles (AVs), identified as single or double membrane-bound vacuoles containing intracellular material (**Fig. 16A,B**). Despite the density of AVs in KD synapses showed a trend of increase, no significantly changes were found (**Fig. 16C**). Regarding the presence of autophagosomes along neurites, we have always been able to detect AVs along neuronal processes in all conditions, but KD neurites were characterized by a significantly increased AV density compared to controls (**Fig. 16D,F**). Notably, the ultrastructural effects of APache KD were reversible: the silencing phenotype was completely rescued by co-transduction of the neurons with eGFP-APache, an overexpressing vector resistant to shRNA silencing (APache rescue) (**Fig. 16A-F**).

Effects of APache downregulation in neurons were also assessed by immunocytochemistry. In silenced samples, LC3 fluorescence intensity, detected in the whole neuron, resulted considerably higher compared to control cells (**Fig. 17A,B**). Moreover, APache KD cells showed a significantly higher colocalization between LC3-positive structures and the synaptic marker VAMP2, compared to controls (**Fig. 17C,D**), with no altered density of synaptic boutons (VAMP2-positive puncta) (**Fig. 17E,F**). These data indicate that, as consequence of APache downregulation, we observe an accumulation of autophagosomes at synapses.

To further confirm autophagic accumulation consequentially to APache silencing, control and KD cortical neurons were also analyzed through western blot assay. APache lacking cells were characterized by significantly higher expression level of LC3 II, indicative of an increased amount of autophagic vacuoles in the cells (**Fig. 17G,H**). Moreover, the expression level of AP-2α resulted also significantly reduced in KD neurons (**Fig. 17G,H**) in agreement with previous results (Piccini et al., 2017).

Collectively, these data demonstrate a strong accumulation of autophagosmes also at synaptic level after APache silencing in neurons.

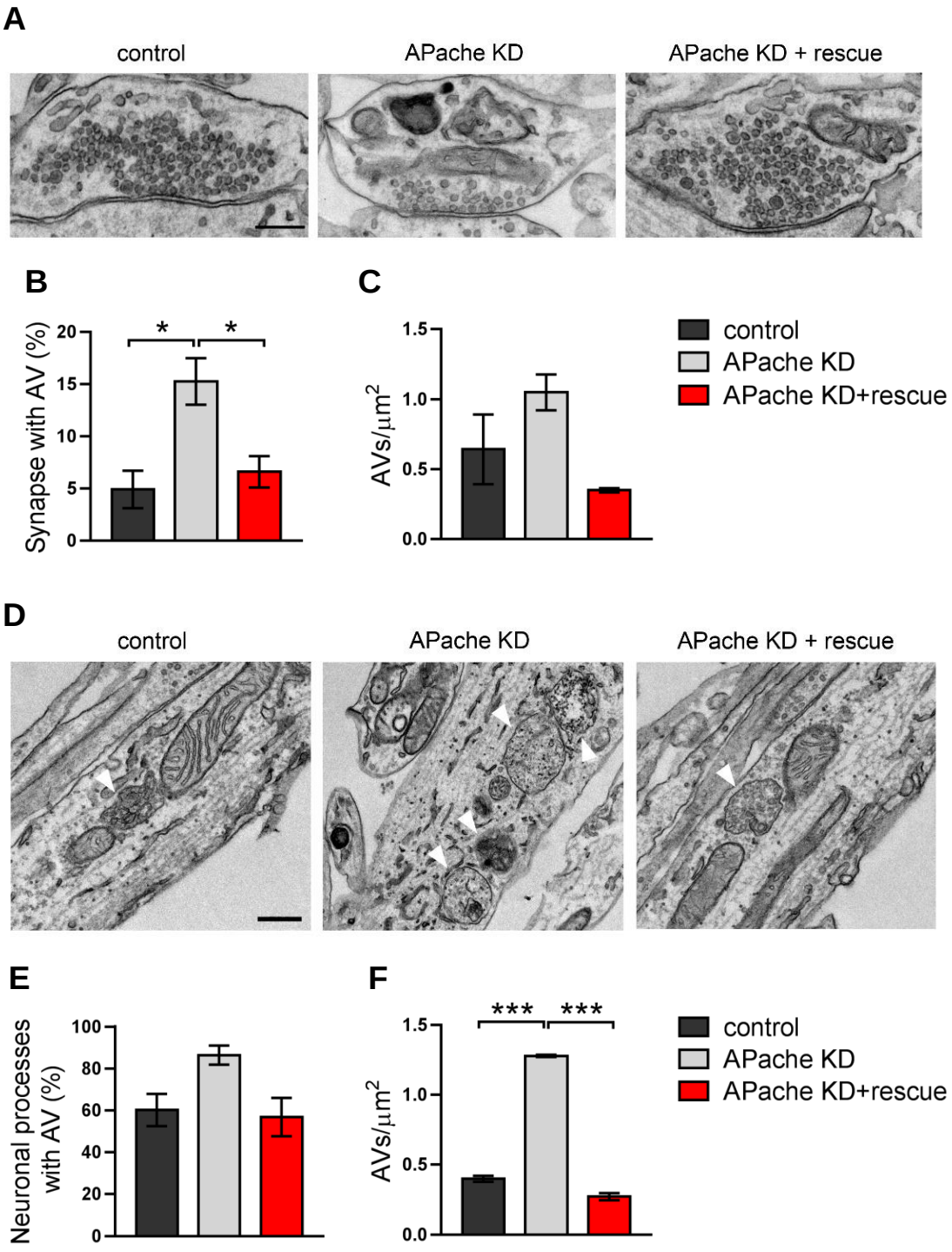
A
control
APache KD
APache KD + rescue
B
Synapse with AV (%)
20
15
10
5
0
*
*
C
AVs/μm2
1.5
1.0
0.5
0.0
control
APache KD
APache KD+rescue
D
control
APache KD
APache KD + rescue
E
Neuronal processes with AV (%)
100
80
60
40
20
0
F
AVs/μm2
1.5
1.0
0.5
0.0
***
***
control
APache KD
APache KD+rescue

**Figure 16: Ultrastructural analysis of autophagic vacuoles in APache KD cortical neurons**

**(A)** Representative electron micrographs of synaptic terminals from cultured cortical neurons transduced at 12 DIV with lentiviral vectors coding for either control mCherry-shRNA (control) or APache mCherry-shRNA (APache KD) and rescued by coinfection with EGFP-APache resistant to silencing (APache rescue), and processed at 17 DIV. Scale bar, 200 nm. **(B,C)** Quantification of the percentage of synapses containing AVs **(B)** and AV density **(C)** in control, APache KD and APache rescue neurons (n=114 control synapses, n=100 APache KD synapses and n=50 APache rescue synapses, from 4 independent preparations). (B: control: 4.897 ± 1.799%, APache KD: 15.278 ± 2.240%, rescue: 6.6 ± 1.5%; C: control: 0.641 ± 0.25, APache KD: 1.05 ± 0.128, rescue: 0.349 ± 0.015). *p<0.05; one-way ANOVA with Bonferroni's multiple comparison test. All graphs show means ± SEM. **(D)** Representative electron micrographs of neurites from control, APache KD or APache rescue cortical neurons. White arrowheads indicate autophagic vacuoles (AV). Scale bar, 200 nm. **(E,F)** Quantification of the percentage of neuronal processes containing AVs **(E)** and AV density **(F)** in control, APache KD and APache rescue neurons (n=54 images per genotype, from 3 independent preparations). (E: control: 60.248 ± 7.687%, APache KD: 86.364 ± 4.545%, rescue: 56.818 ± 9.185%; F: control: 0.4 ± 0.022, APache KD: 1.28 ± 0.008, rescue: 0.272 ± 0.025). ***p<0.001; one-way ANOVA with Bonferroni's multiple comparison test. All graphs show means ± SEM

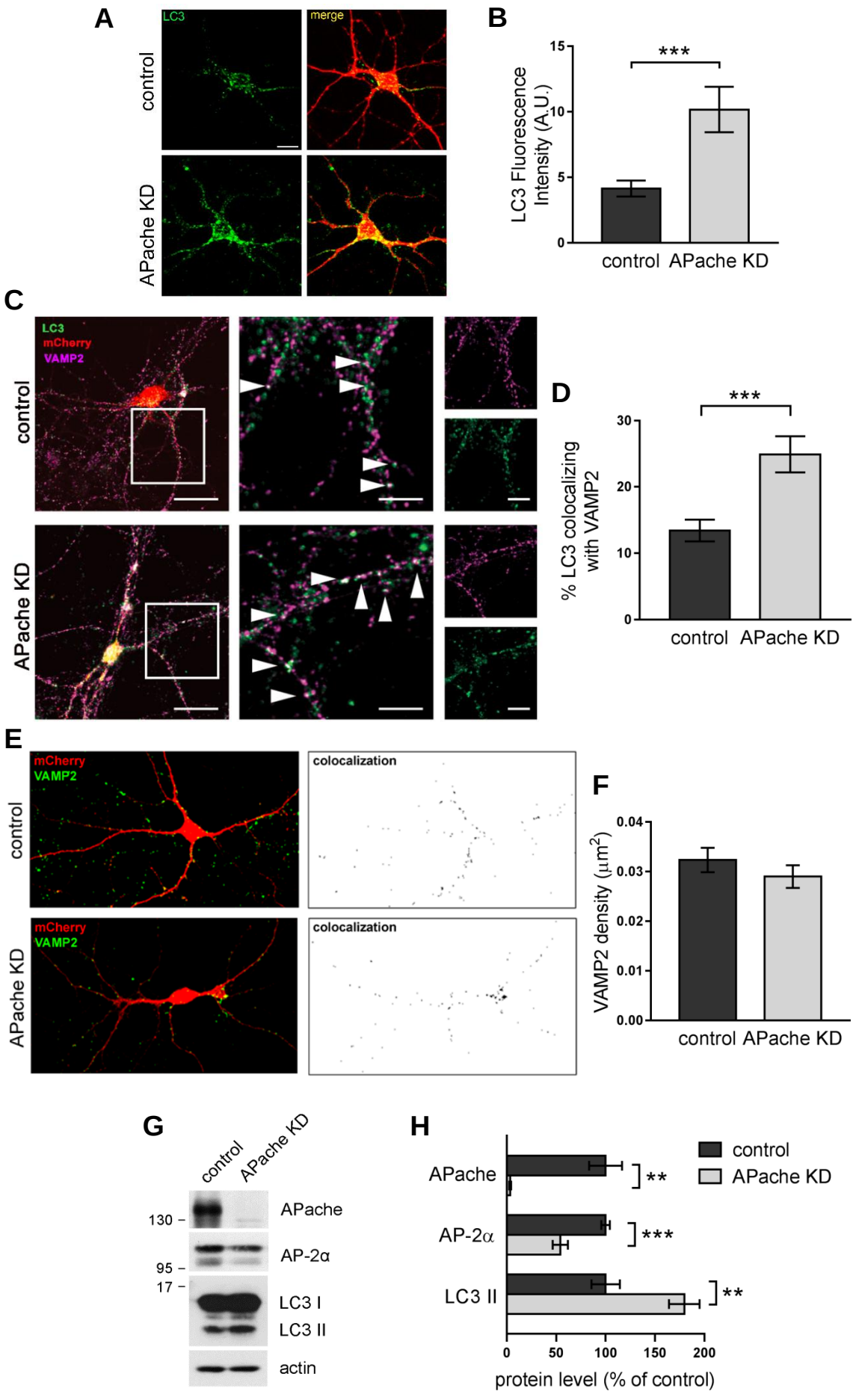
A
LC3
merge
control
APache KD
B
LC3 Fluorescence Intensity (A.U.)
15
10
5
0
***
control
APache KD
C
LC3
mCherry
VAMP2
control
APache KD
D
% LC3 colocalizing with VAMP2
30
20
10
0
***
control
APache KD
E
mCherry
VAMP2
colocalization
control
APache KD
F
VAMP2 density (μm²)
0.04
0.03
0.02
0.01
0.00
control
APache KD
G
control
APache KD
130
95
17
APache
AP-2α
LC3 I
LC3 II
actin
H
control
APache KD
APache
AP-2α
LC3 II
**
***
**
0
50
100
150
200
protein level (% of control)

**Figure 17: APache KD cortical neurons accumulate autophagosomes also at synapses**

**(A)** Representative confocal images of cortical neurons transduced at 12 DIV with lentiviral vectors coding for either control mCherry-shRNA (control) or APache mCherry-shRNA (APache KD) (red) and stained for LC3 (green) at 17 DIV. Scale bar, 10 µm. **(B)** Quantification of LC3 intensity values in control and APache KD neurons (control: 4.14 ± 0.61, n=33 neurons; APache KD: 10.18 ± 1.73, n=31 neurons, from 3 independent preparations). A.U. = arbitrary units of fluorescence intensity. ***p<0.001, Mann-Whitney Unpaired t test. Graph shows means ± SEM. **(C)** Representative confocal images of control or APache KD cortical neurons (red) stained for LC3 (green) and VAMP2 (magenta). White boxes indicate panels magnified to the right. Arrowheads in the magnified inserts indicate points of co-localization between LC3-positive structures and synaptic boutons. Scale bars: 20 µm, 10 µm (inserts). **(D)** Quantification of the percentage of LC3 puncta colocalizing with VAMP2 in control and APache KD neurons (control: 13.42 ± 1.63, n=36 neurons; APache KD: 24.91 ± 2.72, n=38 neurons, from 3 independent preparations). A.U. = arbitrary units of fluorescence intensity. ***p<0.001, Unpaired t test with Welch's correction. Graph shows means ± SEM. **(E)** Representative images of control or APache KD neurons stained for VAMP2 (green). Co-localization panels indicate synaptic boutons of tranduced neurons. Scale bar, 20 µm. **(F)** Quantification of the density of VAMP2-positive puncta in control and APache KD neurons (control: 0.032 ± 0.0024, n=27 neurons; APache KD: 0.029 ± 0.0023, n=28 neurons, from 3 independent preparations). Graph shows means ± SEM. n.s.= non-significant, Mann-Whitney Unpaired T-test. **(G)** Representative western blotting of lysates from cultured cortical neurons transduced at 12 DIV with lentiviral vectors coding for either control mCherry-shRNA (control) or APache mCherry-shRNA (APache KD) and processed at 17 DIV; immunoreaction with antibodies against APache, AP-2α, LC3 II (lower band) and actin, used as loading control. APache is used to confirm its depletion. **(H)** Quantification of APache level (control: 100 ± 16.73; APache KD: 3.4 ± 0.98, n=6 independent preparations), AP-2α level (control: 100 ± 4.37; APache KD: 54.14 ± 7.74, n=6 independent preparations) and LC3 II level (control: 100 ± 14.38; APache KD: 179.7 ± 15.42; n=6 independent preparations). Protein levels in APache KD neurons are expressed in percentage of the respective amounts in control neurons. Values are normalized on loading control. **p<0.01, ***p<0.001, Unpaired t test with Welch's correction. Graph shows means ± SEM.

## 7.3 APache KD neurons accumulate amphisomes

To investigate the molecular mechanism of APache in autophagy, we started by characterizing the nature of autophagosomes that accumulate in neurons consequentially to APache downregulation. During their retrograde transport forward to the soma, autophagosomes may undergo to maturation by fusion with late endosomes to form amphisomes (Wang et al., 2015; Cheng et al., 2015; Maday and Holzbaur, 2016; Kulkarni and Maday, 2018a; Hill and Colón-Ramos, 2020). In order to determinate if APache silenced neurons accumulate newly formed or late-stage autophagosomes, we firstly performed western blot assays on transducted control and KD cortical neurons and measured the expression level of two endosomal Rab proteins associated to different stages of endosomal maturation: Rab5, considered a marker of early endosomes, and Rab7, instead associated to late endosomes. KD neurons showed higher expression levels of Rab7 compared to controls, while Rab5 resulted unchanged between the two conditions (**Fig. 18A,B**), suggesting an increased amount of solely late endosomes/amphisomes in lack of APache.

To visualize late-stage autophagosomes, we then performed immunocytochemistry assays double-labeling control and APache KD cortical neurons for LC3 and Rab7. KD cells showed, in addition to a higher level of fluorescence intensity of LC3 as expected, also increased Rab7 fluorescence intensity compared to controls (**Fig. 18C,D**). Moreover, downregulated cells showed a significantly higher colocalization between Rab7 and LC3 signals (**Fig. 18C,E**), identifying autophagosomes that accumulate in KD neurons are late-stage autophagosomes post-fusion with Rab7-positive late endosomes. Altogether, the biochemical and imaging data argue that the autophagosomal structures observed by electron microscopy have undergone fusion with late endosomes.

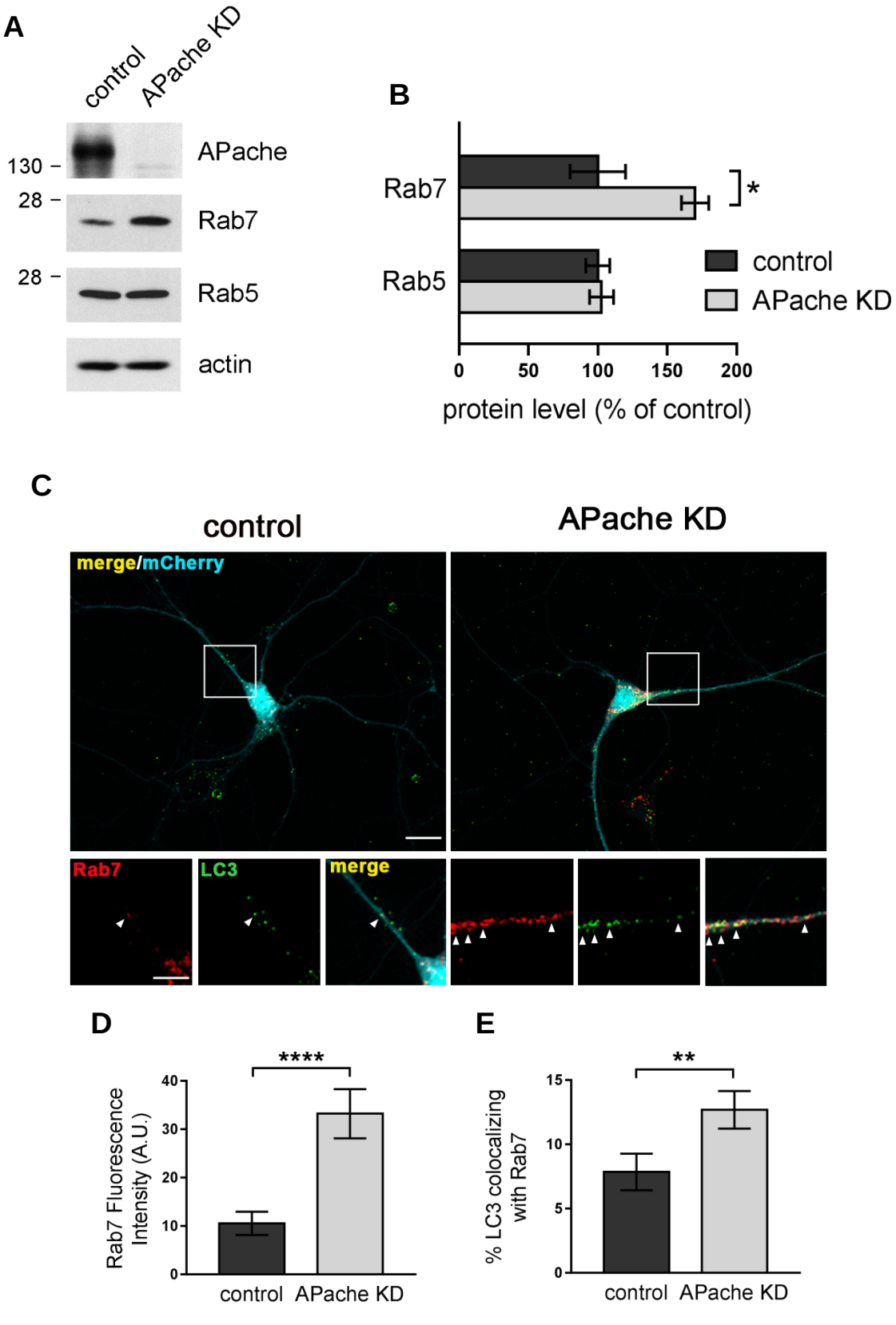
A
control
APache KD
130 –
APache
28 –
Rab7
28 –
Rab5
actin
B
Rab7
Rab5
*
control
APache KD
0
50
100
150
200
protein level (% of control)
C
control
APache KD
merge/mCherry
Rab7
LC3
merge
D
Rab7 Fluorescence Intensity (A.U.)
****
40
30
20
10
0
control
APache KD
E
% LC3 colocalizing with Rab7
**
15
10
5
0
control
APache KD

**Figure 18: Increased amount of late-stage autophagosomes in APache KD cortical neurons.**

**(A)** Representative western blotting of lysates from control or APache KD cortical neurons; immunoreaction with antibodies against APache, Rab5, Rab7 and actin, used as loading control. Rab5 and Rab7 are used as markers of respectively early and late endosomes. **(B)** Quantification of Rab7 level (control: 100 ± 19.91; APache KD: 170.1 ± 9.75, n=6 independent preparations) and Rab5 level (control: 100 ± 8.61; KD: 102.8 ± 8.64; n=6 independent preparations). Protein levels in APache KD neurons are expressed in percentage of the respective amounts in control neurons. Values are normalized on actin levels. Graph shows means ± SEM. *p<0.05, Unpaired t test with Welch's correction. **(C)** Representative confocal images of control or APache KD cortical neurons (blue) stained for LC3 (green) and Rab7 (red). Channels were false color-coded to better illustrate the co-localization. White boxes indicate panels magnified to the right. Arrows in the magnified inserts indicate points of co-localization between LC3 and Rab7 along neurites. Scale bars: 10 µm, 5 µm (inserts). **(D)** Quantification of Rab7 intensity values in control and APache KD neurons (control: 10.55 ± 2.40, APache KD: 33.24 ± 5.09, n=31 neurons from 3 independent preparations). A.U. = arbitrary units of fluorescence intensity. **(E)** Quantification of the percentage of LC3 puncta colocalizing with Rab7 in control and APache KD neurons (control: 7.84 ± 1.41, APache KD: 12.68 ± 1.46, n= 31 neurons from 3 independent preparations). All graphs show means ± SEM. **p<0.01, ****p<0.0001; Mann-Whitney Unpaired t test.

## 7.4 APache silencing causes the blockade of the autophagic flux

Once assessed APache participation in autophagy pathway, we wanted to define its molecular mechanism starting by the identification of the autophagic stage in which APache is involved. Autophagy is a complex process and requires a strictly regulation during all its phases. Thus, alterations in every step of the pathway lead to an important unbalancing between autophagosome formation and degradation. Autophagosome accumulation is indeed mainly imputable to two factors: a greater autophagic production, or a blockade of the cycle with a consequential diminished autophagic degradation (Zhang et al., 2013; Mizushima and Murphy, 2020). Our electron microscopy, fluorescence microscopy and biochemical analysis showed a strong accumulation of autophagosomal structures that have undergone fusion with late endosomes all over APache KD neurons, along neurites and at presynaptic terminals. But the increased level of LC3 II that we observed does not necessarily estimate the autophagic activity, because not only autophagy activation but also inhibition of autophagosome degradation greatly increases the amount of LC3 II.

For this reason, we focused on the early stages of autophagy: induction and autophagosome formation. We analyzed lentiviral transducted control and APache KD cortical neurons through western blot by measuring the expression level of crucial mediators of autophagic induction and formation. To evaluate the level of induction of the autophagyc cycle, we analyzed the level of the main autophagic regulator mTOR, in both its total and active form phospho-mTOR. To monitor the generation of new autophagosomes we measured the level of two proteins required for autophagosome formation, Atg 3 and Atg5. Western blot analysis reported no differences between control and silenced neurons in the level of mTOR/phosphor-mTOR, as well as Atg proteins (**Fig. 19A,B**), excluding alterations in the early stages of autophagy consequentially to APache downregulation.

Degradation of the autophagic receptor p62 is a widely used marker to monitor autophagy activity, because p62 directly binds to LC3 and is selectively degraded by autophagy (Bjørkøy et al., 2005; Zhang et al., 2013; Mizushima et al., 2020). We then tested control and APache KD cortical neurons to assess if the alterations observed in silenced cells were caused by a blockade of the autophagic flux. We analyzed the samples through immunocytochemistry and detected the signal of p62. Silenced neurons showed a significantly increase in p62 fluorescence intensity compared to

control neurons (**Fig. 19C,D**), indicative of a blockade of the autophagic flux in the absence of APache.

To estimate autophagosome maturation and degradation further, we used a version of LC3 probe tagged with both eGFP and the red fluorescent protein mCherry (mCherry-eGFP-LC3B). Both fluorescent reporters are active before fusion and acidification of autophagosome with lysosome, making immature autophagosomes emit both green and red signals, and appear yellow. The eGFP signal is quenched when autophagosome acidifies, because of the degradation of eGFP by lysosomal proteases, while the mCherry is unaffected, so mature autolysosomes appear exclusively red. The dynamic switch from yellow to red fluorescence its indicative of a functional autophagic flux process. Accordingly, when the autophagy flux is blocked and the formation of autolysosomes is impaired, the ratio between the green and the red signal increases (Mizushima and Murphy, 2020).

We cotransfected mouse cortical neurons at 14 DIV with the tandem mCherry-eGFP-LC3B construct and control or APache silencing vectors (mTurquoise-ShRNA), and we imaged the cells soma at 17 DIV to detect the signal of both mCherry and eGFP. The calculated eGFP/mCherry intensity ratio resulted significantly higher in silenced cells compared to control neurons (**Fig. 19E,F**), confirming the autophagic blockade consequentially to APache downregulation.

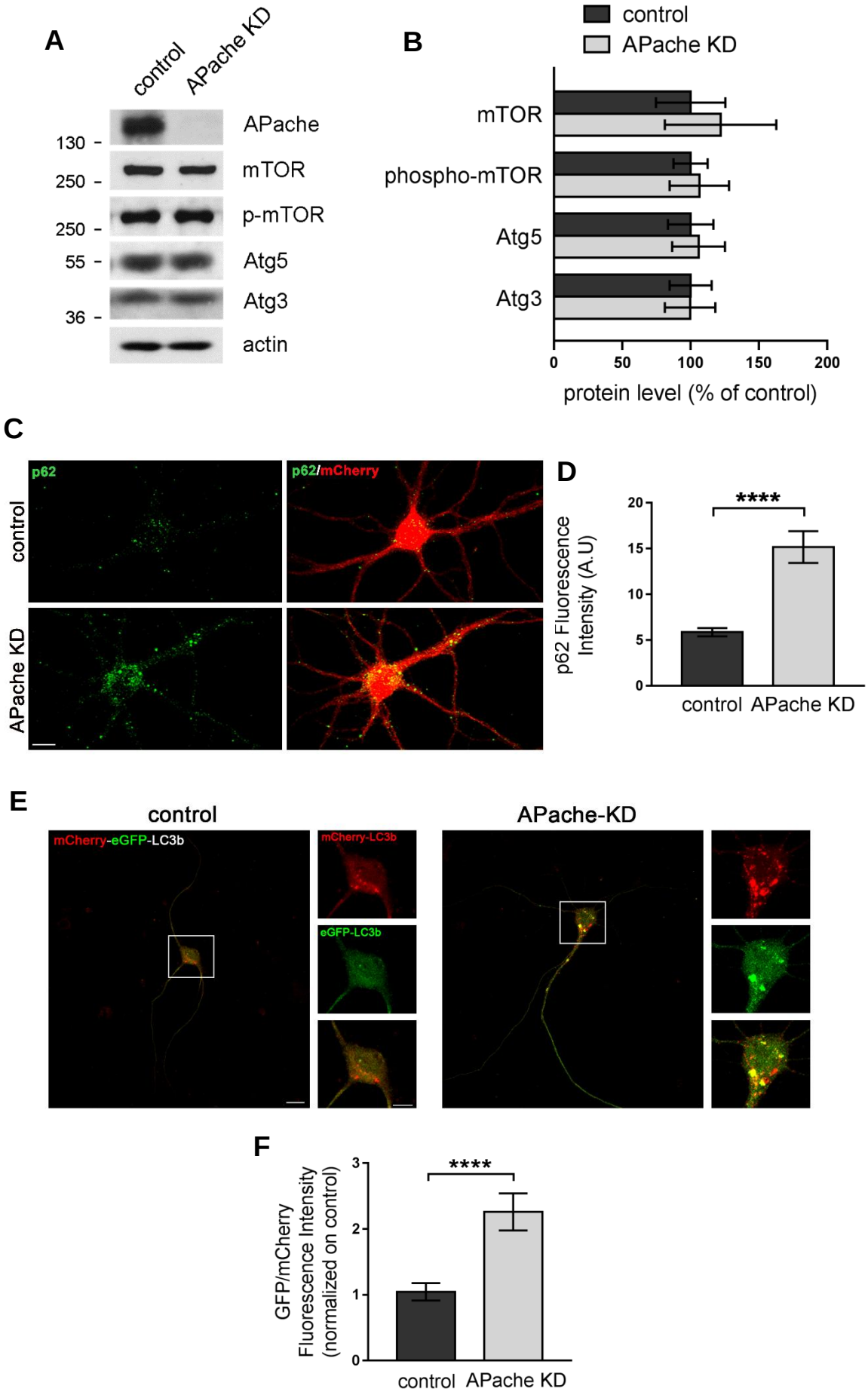
A
control
APache KD
130
250
250
55
36
APache
mTOR
p-mTOR
Atg5
Atg3
actin
B
control
APache KD
mTOR
phospho-mTOR
Atg5
Atg3
0
50
100
150
200
protein level (% of control)
C
p62
p62/mCherry
control
APache KD
D
p62 Fluorescence Intensity (A.U)
****
20
15
10
5
0
control
APache KD
E
control
APache-KD
mCherry-eGFP-LC3b
mCherry-LC3b
eGFP-LC3b
F
GFP/mCherry Fluorescence Intensity (normalized on control)
****
3
2
1
0
control
APache KD

**Figure 19: APache silencing causes the blockade of autophagic flux.**

**(A)** Representative western blotting of lysates from control or APache KD cortical neurons; immunoreaction with antibodies against APache, mTOR, phospho-mTOR(Ser2448) (p-mTOR), Atg5, Atg3 and actin, used as loading control. APache is used to verify the actual silencing of the protein. mTOR and phospho-mTOR are used to evaluate the level of autophagy induction. Atg5 and Atg3 are used as markers of early autophagosomes **(B)** Quantification of mTOR level (control: 100 ± 25.46; APache KD: 121.9 ± 40.81), p-mTOR level (control: 100 ± 37.41; KD: 106.4 ± 21.77), Atg5 level (control: 100 ± 16.67; APache KD: 105.8 ± 19.38) and Atg3 level (control: 100 ± 15.35; APache KD: 99.57 ± 18.52). n=6 from 3 independent preparations. Protein levels in APache KD neurons are expressed in percentage of the respective amounts in control neurons. Values are normalized on actin levels. Graph shows means ± SEM. Unpaired t test with Welch's correction. **(C)** Representative confocal images of control or APache KD cortical neurons (red) stained for p62 (green). Scale bar, 20 µm. **(D)** Quantification of p62 intensity values in control and APache KD neurons (control: 5.85 ± 0.45, n=34 neurons; APache KD: 15.17 ± 1.74, n=37 neurons, from 3 independent preparations). ****p<0.0001. Mann-Whitney Unpaired t test. A.U. = arbitrary units of fluorescence intensity. **(E)** Representative confocal images of mouse cortical neurons (17 DIV) co-transfected at 14 DIV with vectors coding for either control mTurquoise-shRNA (control) or APache mTurquoise-shRNA (APache KD) and tandem mCherry-eGFP-LC3B, as a reporter of autolysosome formation. White boxes indicate soma shown magnified to the right. Scale bar, 20 µm (10 µm in the insets). **(F)** Mean eGFP/mCherry intensity ratio in control and APache KD neurons (control: 0.9861 ± 0.1692, n=44 neurons; APache KD: 1.997 ± 0.2414, n=45 neurons, from 5 independent preparations). All graphs show means ± SEM. ****p<0.0001 Dunn's multiple comparisons test.

## 7.5 APache silencing does not alter lysosomal density and functionality

A block in autophagy leads to a decreased degradation of autophagosomes, that accumulate within the neuron. The cause of this impaired clearance may depend on an inefficient transport of autophagosomes to the soma, an altered fusion with lysosomes and/or to lysosomal dysfunctions (Kononenko et al., 2017; Tamminemi et al., 2017; Whyte et al., 2017; Bingol, 2018).

To identify the cause of the autophagic block in APache KD neurons, we first focused on lysosomes. The two main factors impacting on lysosomal degradation usually are represented by a low number of lysosomes, insufficient to cope with autophagosome production, or the presence of dysfunctional lysosomes with a diminished proteolytic activity (Trivedi et al., 2020).

We first evaluated lysosomal density in control and APache KD cortical neurons silenced through lentiviral transduction, by measuring through immunocytochemistry the fluorescence intensity of the lysosomal marker LAMP1. LAMP1 signal resulted similar in both controls and silenced cells (**Fig. 20A,B**). To confirm the result, we measured the expression level of LAMP1 in control and KD neurons by performing western blot analysis. Similarly to immunofluorescence result, control and KD samples showed similar levels of LAMP1 (**Fig. 20C,D**). These data indicate that APache silencing does not affect lysosomal density.

In light of this data, we focused on lysosomal functionality, which relies on the enzymatic activity of hydrolases, mainly represented by cathepsins (Roberts, 2005). To evaluate lysosomal degradative activity, we first measured by western blot analysis the expression level of the lysosomal enzyme cathepsin D (CTSD) in transducted APache KD cortical neurons, to evaluate if APache silencing could alter the concentration of this enzyme. KD cells showed a similar CTSD expression level compared to controls (**Fig. 20C,D**). To test the functionality of this enzyme, we performed a colorimetric assay to measure the proteolytic activity in cell lysates obtained from both control and transducted APache KD cortical neurons. The enzyme resulted equally active in both control and KD samples (**Fig. 20E**).

Moreover, the expression level of ATP6V1A, the A subunit of the protonic pump vATPase that acidifies lysosomes, identified as an APache interactor (Piccini et al., 2017), resulted unaltered in silenced neurons compared to control cells (**Fig. 20C,D**).

Collectively, these data exclude an altered lysosomal density and degradative activity as putative cause for autophagosome accumulation observed in APache KD neurons, suggesting that APache role in autophagy relies on other mechanisms of the pathway.

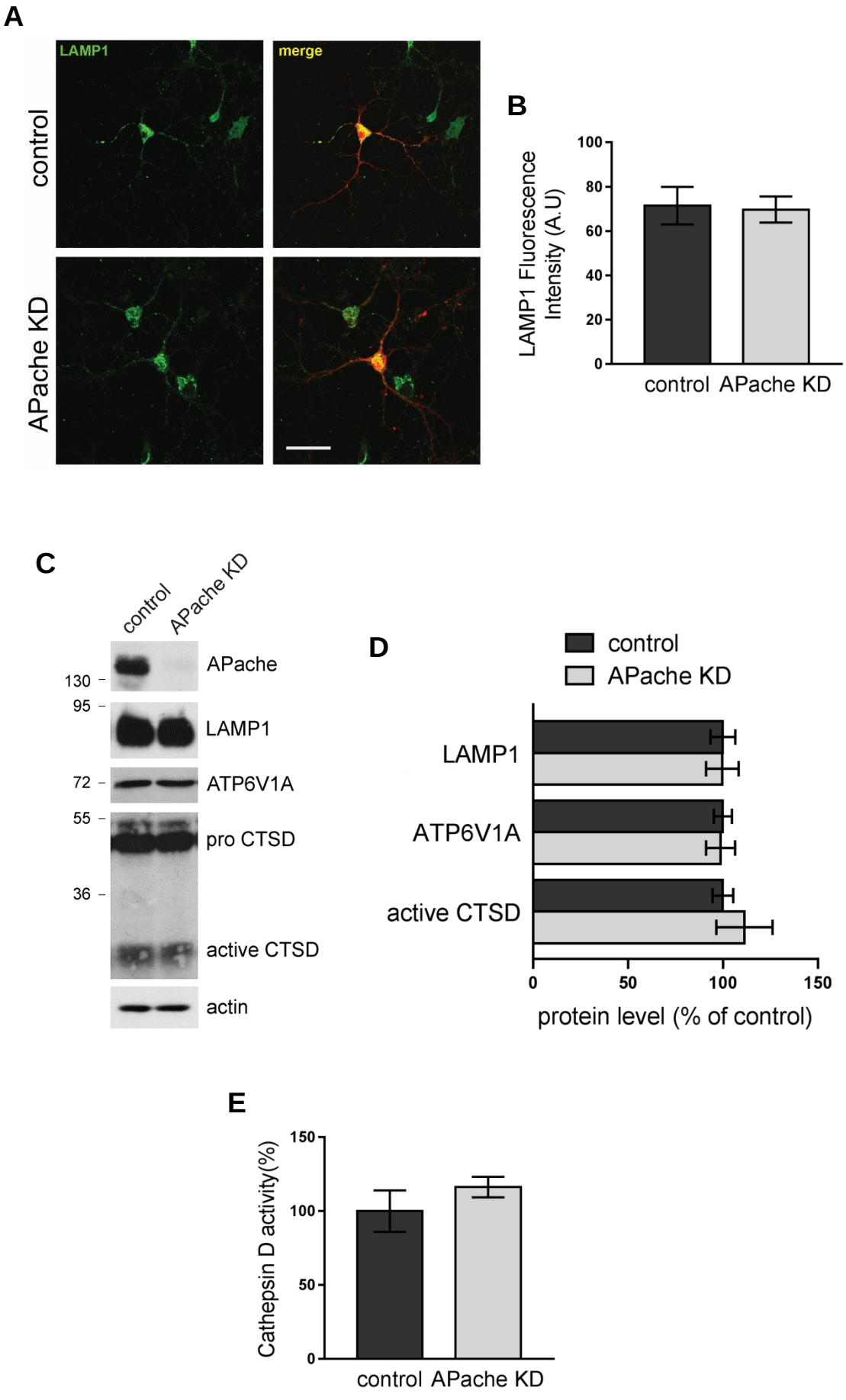
A
LAMP1
merge
control
APache KD
B
LAMP1 Fluorescence Intensity (A.U)
100
80
60
40
20
0
control
APache KD
C
control
APache KD
130
95
72
55
36
APache
LAMP1
ATP6V1A
pro CTSD
active CTSD
actin
D
control
APache KD
LAMP1
ATP6V1A
active CTSD
0
50
100
150
protein level (% of control)
E
Cathepsin D activity(%)
150
100
50
0
control
APache KD

**Figure 20: APache silencing does not alter lysosomal density and functionality.**

**(A)** Representative confocal images of control or APache KD neurons (red) stained for the lysosomal marker LAMP1 (green). Scale bar, 20 µm. **(B)** LAMP1 intensity values in APache KD neurons are unaltered compared to control neurons (control: 71.46 ± 8.44, APache KD: 69.70 ± 5.87, n=24 neurons, from 3 independent preparations). A.U. = arbitrary units of fluorescence intensity. Unpaired t test with Welch's correction. **(C)** Representative western blotting of lysates from control or APache KD cortical neurons; immunoreaction with antibodies against LAMP1, ATP6V1A, cathepsin D (total form: pro CTSD; active form: active CTSD) and actin, used as loading control. **(D)** Quantification of LAMP1 level (control: 100 ± 6.57; APache KD: 99.71 ± 8.59, n=10 from 4 independent preparations), active CTSD level (control: 100 ± 5.45; APache KD: 111.4 ± 14.87, n=7 from 3 independent preparations) and ATP6V1A level (control: 100 ± 4.8; KD: 98.78 ± 7.69; n=5 from 2 independent preparations). Protein levels in APache KD neurons are expressed in percentage of the respective amounts in control neurons. Values are normalized on actin levels. All graphs show means ± SEM. Unpaired t test with Welch's correction. **(E)** Cathepsin D activity in control and APache KD neurons. Data were normalized to µg protein/sample and expressed in percentage of control values (control: 100 ± 14.03; APache KD: 116 ± 6.97, n=8 samples from 3 independent preparations). Graph shows means ± SEM. Unpaired Student’s t test.

## 7.6 APache silencing does not alter autophagic retrograde transport

One of the major events driving neuronal autophagy consists in retrograde transport of autophagosomes from synapses to the soma, where most lysosomes are located, along axonal microtubules, through an active process that requires the mediation of the motor complex dynactin (Wang et al., 2015; Cheng et al., 2015; Kulkarni and Maday, 2018b; Hill and Colón-Ramos, 2020). Neurons with an impaired autophagic transport are characterized by an accumulation of AVs at synapses and along the axon (Boland et al., 2008; Nixon and Yang, 2011; Kononenko et al., 2017).

To test if an inefficient autophagosome retrograde transport may contribute to autophagic accumulation observed in APache-silenced neurons, we monitored autophagosome transport in mouse cortical neurons through live-cell imaging. Neurons were cotransfected at 10 DIV with control or APache-silencing eEGFP-ShRNA-vectors and RFP-LC3B construct, and at 13 DIV RFP-tagged autophagosomes were tracked along axons to evaluate their motility (**Fig. 21A**). To better visualize the movements of LC3 puncta during the recordings, the analyzed axonal tracts were represented by kymographs, graphical illustrations commonly used to provide the spatial position of particles over time (**Fig. 21B**).

Axonal tracts around 25 μm of length were imaged for 30 s, and recordings were analyzed to calculate the fraction of stationary versus mobile autophagosomes (in retrograde direction or anterograde behavior). Afterward, retrograde moving RFP-puncta were manually tracked to measure their velocity (μm/s). In control and APache KD neurons the percentage of retrograde autophagosomes over the total LC3 puncta population resulted unchanged (control: 11 ± 1.53%; APache KD: 6.33 ± 1.86%) (**Fig. 21C**), as well as the velocity of retrograde autophagosomes in KD neurons resulted similar to control neurons (control: 0.3 ± 0.04 μm/s; APache: 0.31 ± 0.04 μm/s) (**Fig. 21D**).

Currently, these findings indicate that APache silencing does not alter autophagosome mobility, neither in terms of number of retrograde organelles nor in their velocity. However, this must be considered a preliminary result, as until now we performed a limited number of experiments, still insufficient to draw firm conclusions on APache role in autophagosome trafficking.

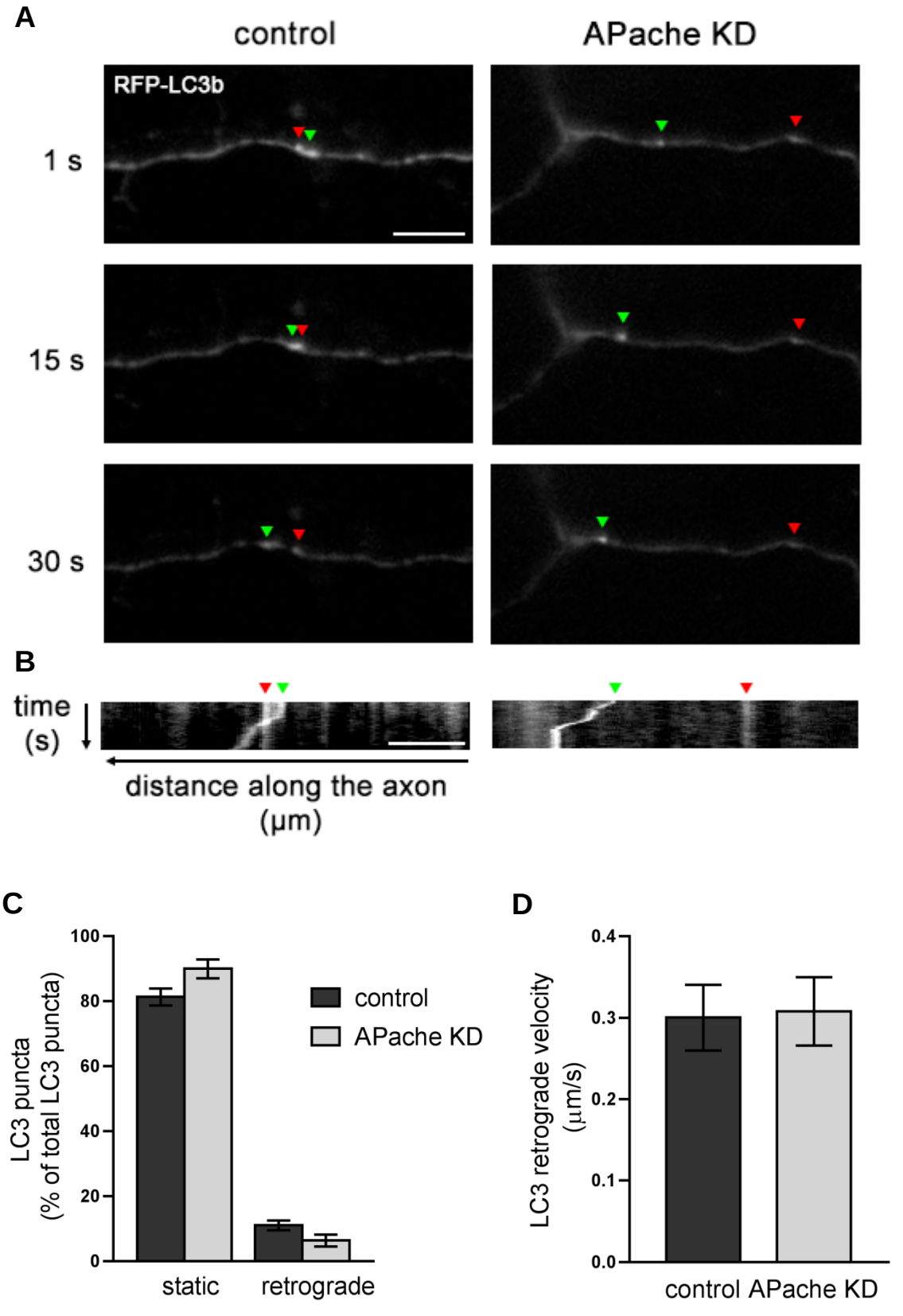
A
control
APache KD
RFP-LC3b
1 s
15 s
30 s
B
time (s)
distance along the axon (μm)
C
LC3 puncta (% of total LC3 puncta)
100
80
60
40
20
0
control
APache KD
static
retrograde
D
LC3 retrograde velocity (μm/s)
0.4
0.3
0.2
0.1
0.0
control
APache KD

**Figure 21: APache silencing does not alter autophagic retrograde transport**

**(A,B)** Representative time-lapse images (0 s, 15 s, 30 s) **(A)** and corresponding kymographs **(B)** of mouse cortical neurons (13 DIV) co-transfected at 10 DIV with vectors coding for either control eEGFP-shRNA (control) or APache eEGFP-shRNA (APache KD) and RFP-LC3b as a reporter of autophagosomes. Arrowheads indicate static (red) and retrograde (green) LC3 puncta (white). Scale bars, 5 µm. **(C, D)** Quantification of stationary and retrograde LC3 puncta expressed in percentage of total LC3 puncta **(C)** (control: static: 81.33 ± 2.6%, retrograde: 11 ± 1.53%; APache KD: static: 90 ± 2.89%, retrograde: 6.33 ± 1.86%, n=3 independent preparations) and relative retrograde velocity **(D)** (control: 0.3 ± 0.04 µm/s, n=40 LC3 puncta; APache: 0.31 ± 0.04 µm/s, n=20 LC3 puncta, from 3 independent preparations). All graphs show means ± SEM. Two-way ANOVA/Mann-Whitney Unpaired t test.

## 7.7 AD human brains show reduced APache expression

Alterations in autophagy link to several neurodegenerative diseases, such as AD, where neurons are characterized by a severe accumulation of autophagosomes (Boland et al., 2008; Nixon and Yang, 2011). Functional alterations of the endosomal and autophagic pathways and of SV trafficking occur as early pathogenic events in AD neurons (Cao et al., 2010). This distinctive phenotype resembles the one we observed in APache KD neurons and the one reported in AP-2 KO neurons, a protein playing a role in neuronal autophagy preventing neurodegeneration (Kononenko et al., 2017; Bera et al., 2020).

In light of this morphological similarity, considered the previously described thigh connection between APache and autophagy, we wanted to indagate if APache is involved in the pathogenesis of the precocious neuronal alterations observed in AD that directly contribute to synaptic dysfunction and reduced neuronal survival. To test this hypothesis, we measured by western blot analysis the expression level of APache in autopsy sections from frontal cerebral cortex of late onset sporadic AD patients and cognitively normally aging elderly subjects as controls (aged matched). Synaptic integrity was checked measuring the expression level of the synaptic marker synaptotagmin 1 (Syt 1). AD brains showed a drastically decreased expression level of APache compared to controls (**Fig. 22A,B**), not imputable to neuronal loss or synaptic degeneration, since level of Syt 1 was unchanged (**Fig. 22A,B**). Notably, also the level of AP-2 was significantly reduced in AD brain samples (**Fig. 22A,B**).

We are currently evaluating whether APache silencing might contribute to the pathogenesis of AD by modifying the processing of amyloid precursor protein APP and production of Aβ. Preliminary results obtained by western blot analysis on extracellular soluble APP levels (sAPP), as a read-out of the general cleavage of the protein, showed a reduction of extracellular sAPP levels in cell medium of APache KD neurons compared to controls (data not shown).

These data indicate that APache may be involved in the pathogenesis of AD and it may represent a useful marker to monitor the progression of the disease at early stages, when neuronal death is not already occurred.

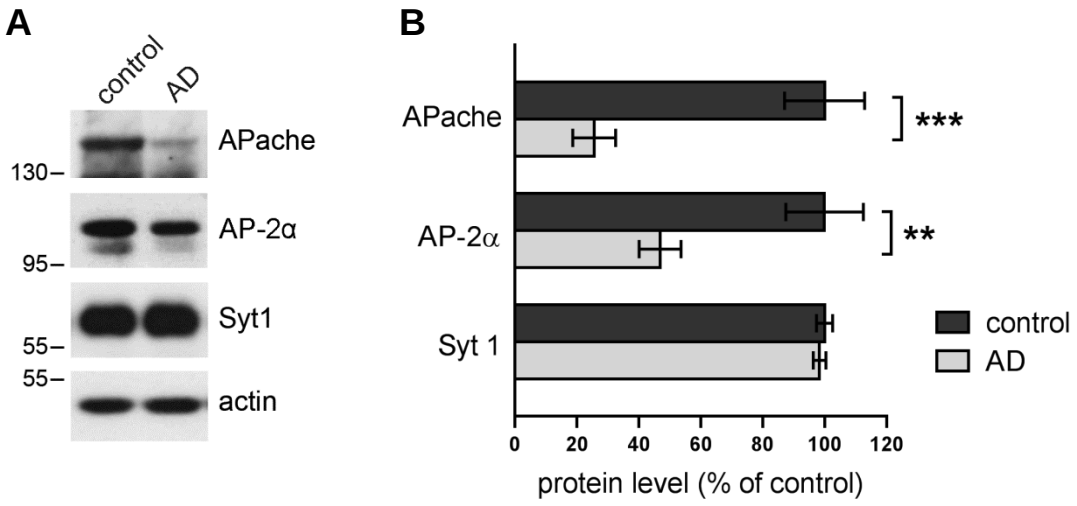


**Figure 22: Decreased APache protein level in human AD brains**

**(A)** Representative western blotting of homogenates from brain samples of late onset sporadic AD patients (AD) and cognitively normally aging elderly subjects (control); immunoreaction with antibodies against APache, AP-2$\alpha$, synaptotagmin 1 (Syt 1) and actin. Syt 1 is used as synaptic markers to evaluate synaptic loss. Values are normalized on Sy 1 levels. **(B)** Quantification of APache level (control: 100 ± 12.95; AD: 25.62 ± 6.92), AP-2$\alpha$ level (control: 100 ± 12.54; AD: 46.87 ± 6.75) and Syt 1 level (control: 100 ± 2.56; AD: 98.4 ± 2.05), n=8 subjects per condition. Protein levels in AD brains are expressed in percentage of the respective amounts in control brains. Values are normalized on Syt 1 levels. **p<0.01, ***p<0.001, Unpaired Student's t test/Mann-Whitney Unpaired test. All graphs show means ± SEM.

# 5. Discussion

Autophagy is a highly conserved self-eating process fundamental for the regulation of cellular homeostasis by eliminating old or damaged cell components to obtain basic metabolites during stress or starvation (Debnath et al., 2005; Reef et al., 2006). Considering that neurons are perennial polarized cells subjected to high constant activity for neurotransmission, the proper clearance of dysfunctional components through autophagy results particularly crucial (Vijayan and Verstreken, 2017; Wang et al., 2017). To date it is clear that several presynaptic proteins canonically known for their role in SV endocytosis, such as AP-2 (Kononenko et al, 2017; Azarnia Tehran et al., 2018; Overhoff et al., 2020), play also a role in autophagy and neurodegeneration. In fact, alterations in any step of autophagy link to several neurodegenerative diseases (Nixon et al., 2013; Frake et al., 2015; Menzies et al., 2015; Azarnia Tehran, 2018; Bingol, 2018; Fujikake et al., 2018; Overhoff et al., 2020). For this reason, in the last decade several studies focused on the characterization of neuronal autophagy, a process still largely unclear especially as regards the molecular players involved, highlighting the necessity of identification of neuronal specific autophagic markers.

In this study, we investigated the involvement of APache in neuronal autophagy. APache is a previously unknown protein identified as a novel interactor of AP-2 and characterized in our research group as an important actor in CME playing an essential role in neuronal development and synaptic transmission. Pull-down experiments and mass spectrometry analysis identified several proteins involved in organelle/vesicular transport, part of the endosomal and lysosomal systems, as APache-interacting partners (Piccini et al., 2017; **Fig. 12** Introduction).

The involvement of APache in neuronal autophagy has been suggested by the strong increase of its protein level observed in primary cortical neurons after autophagy stimulation with Torin1 also at synaptic level, and by the increased colocalization between APache and LC3 at the level of autophagosomes in this condition (**Fig. 14** Results). The data were corroborated by APache enrichment at the level of the membrane/organellar fraction of the neurons, where also autophagosomes and autolysosomes are enriched (**Fig. 15** Results). These results suggest that APache may be present at level of autophagosome membranes and participate to autophagic

pathway. Experiments of co-immunoprecipitation of APache and LC3 performed in mouse brain extracts did not reveal a direct interaction between the two proteins (data not shown), and a purification of autophagomes will be therefore needed to validate APache association with these vacuolar structures.

Several lines of evidence suggest that APache is not simply involved, but even crucial for the normal proceeding of the autophagic cycle. In distal axon autophagosomes fuse with late endosomes to form amphisome (Cheng et al. 2018; Yap et al. 2018) and begin a process of maturation that is coupled with their retrograde transport mediated by dynactin through axonal microtubules toward the cell body, where lysosomes are enriched, and fuse with lysosomes allowing their degradation (Wang et al., 2015; Cheng et al., 2015; Kulkarni and Maday, 2018b). Western blot analysis, fluorescence and electron microscopy revealed a defective autophagy in neurons after APache silencing (**Fig. 16, 17** and **18** Results). We observed a severe accumulation of autophagic structures, mainly late-stage autophagosomes, already fused with late endosomes, along neurites and at presynaptic terminals in absence of APache. A blockade of the autophagic flux leading to a consequential accumulation of autophagosomes (Mizushima & Murphy, 2020; Zhang et al., 2013) was demonstrated by increased autophagic receptor p62 level and mCherry-eGFP-LC3B switch from red to yellow fluorescence observed in APache-silenced neurons (**Fig. 19** Results). Unaltered expression levels of crucial mediators of autophagy induction (phospho-mTOR) and formation (Atg3 and Atg5) in absence of APache (**Fig. 19** Results) instead excluded an involvement of the protein in the early stages of the pathway.

The precise molecular mechanism causing the blockade of the autophagic flux after APache silencing in neurons is unfortunately still lacking. AP-2 is an important mediator of autophagosome retrograde transport, by binding both LC3 and the motor complex dynactin (Kononenko et al., 2017). In light of APache direct interaction with AP-2 (Piccini et al., 2017), we speculated that together with AP-2 APache might be part of a protein complex that mediates autophagosome retrograde transport. Unexpectedly, APache seems not involved in the retrograde transport of autophagosomes to the soma: in absence of APache the amount of autophagosomes moving through retrograde transport and also their velocity were similar to what we observed in control conditions (**Fig. 21** Results). Moreover, analysis performed through fluorescence microscopy and biochemical assays (**Fig. 20** Results) revealed that APache-silenced neurons have no alterations neither in the amount of the main lysosomal marker LAMP1 and ATP6V1A (the A subunit of the protonic pump vATPase that acidifies lysosomes identified as an APache interactor) nor in the expression and activity of the

lysosomal hydrolase cathepsin D, to indicate that APache silencing does not affect lysosomal density and degradative activity.

The implication of APache-AP2 interaction, if any, in the autophagic context remains still unclear. Certainly, our data showed a close correlation between the levels of both proteins: with the induction of autophagy in neurons with Torin1 both levels are increased (**Fig. 14** Results), in APache-silenced neurons AP-2 levels are roughly halved (**Fig. 15** Results), in brain samples of AD we observed a drastic reduction in the expression levels of both proteins (**Fig. 22** Results). Beyond a close functional correlation, there could be a role of APache in determining the stability of AP-2 in the formation of a molecular complex.

Synapses represent a key site in neuronal autophagy: both autophagic induction and autophagosome formation occurs at synaptic boutons (Wang et al., 2015; Cheng et al., 2015; Kulkarni and Maday, 2018b) and autophagy itself influences synaptic morphology and functioning (Hernandez et al., 2012; Vijayan and Verstreken, 2017). Moreover, AD neurons are characterized by a distinctive accumulation of AVs at presynaptic terminals caused by autophagic alterations (Boland et al., 2008; Nixon and Yang, 2011). We assessed a strong autophagic accumulation at APache-silenced synapses, and, moreover, biochemical analysis performed on brain samples of late onset sporadic AD patients showed a severely decreased level of APache at early stages of the disease, when synaptic loss is not already occurred (**Fig. 22** Results). Levels of several proteins involved in SV trafficking are reduced from early stages of the disease and are associated with ultrastructural changes and impaired function of the synapses (Cao et al., 2010; Yao et al., 2003; Masliah et al., 2001). We can speculate that APache function is defective in AD and this is causally related to pathological neuronal alterations in SV and autophagy trafficking. Future studies will be needed to verify this hypothesis, but the possible involvement of APache also at synaptic levels would broaden our knowledge about new neuronal-specific autophagic markers useful for the identification of new drug targets.

# 6. Conclusions and future perspective

In this dissertation we described APache as a novel presynaptic actor of autophagy, involved in the mid and late stages of the pathway. We showed that APache downregulation causes a blockade of the autophagic flux, with a consequential accumulation of late-stage autophagosomes that occurs in the whole neuron, along neurites and at presynaptic terminals. The precise molecular mechanism of APache is still unknown, however our data indicate that the autophagic blockade observed in APache KD neurons is not due to alterations in lysosomal density or dysfunctional lysosomal enzymes.

Interestingly, APache level resulted severely reduced in brain samples of late onset sporadic AD patients when synaptic loss is not already occurred. We speculate that an altered APache level or a perturbation of its function may contribute to the pathogenesis of the precocious neuronal alterations observed in AD. A clearer elucidation of its functional role in neurons, therefore, may provide useful insight into the pathogenetic mechanisms at the basis of this untreatable disease, and is attractive and promising for the identification of druggable targets, which are urgently needed to achieve a definitive therapy for AD. Moreover, the main markers used to evaluate autophagic activity have a wide expression, not limited to the neural tissue (e.g. LC3), thus, the identification of a neuron-specific autophagic marker is still an important challenge researchers are dealing with. The neuron-specific expression of APache raises the intriguing possibility that this protein may be a promising candidate marker to specifically monitor neuronal autophagy.

To characterize the molecular mechanism of APache in neuronal autophagy, further experiments are still needed. We plan to conclude preliminary experiments on autophagosome trafficking and we are currently further analyzing lysosomal function by evaluation of EGF-induced degradation of EGF receptor in control and APache-silenced neurons. We will investigate the fusion between autophagosomes and lysosomes, a crucial step of autophagy essential to guarantee the proper clearance of autophagosomes. In particular, we will focus on the interaction between autophagic and lysosomal SNARE proteins by performing co-immunoprecipitation or pull-down binding assays.

# 7. Acknowledgments

I would like to express my gratitude to all the people supporting me during my PhD.

First, I want to thank my supervisor prof. Silvia Giovedì for her guidance and help in developing this project, and prof. Fabio Benfenati for the precious suggestions.

I want to give a great acknowledgment to Alessandro Esposito, Enrico Castroflorio and Mattia Bramini, for their essential support in electron and confocal microscopy experiments.

A special thank goes to the “DIMES clan”, all my colleagues, lab mates and friends who made my PhD a stimulating and enjoyable experience through constant advices, intriguing ideas and, above all, the countless funny moments we shared together.

# 8. References


Andres-Alonso M, Ammar MR, Butnaru I, Gomes GM, Acuña Sanhueza G, Raman R, Yuanxiang P, Borgmeyer M, Lopez-Rojas J, Raza SA, Brice N, Hausrat TJ, Macharadze T, Diaz-Gonzalez S, Carlton M, Failla AV, Stork O, Schweizer M, Gundelfinger ED, Kneussel M, Spilker C, Karpova A, Kreutz MR. “SIPA1L2 controls trafficking and local signaling of TrkB-containing amphisomes at presynaptic terminals”. Nat Commun. 2019 Nov 29;10(1):5448. doi: 10.1038/s41467-019-13224-z. PMID: 31784514; PMCID: PMC6884526.

Azarnia Tehran D, Kuijpers M, Haucke V. “Presynaptic endocytic factors in autophagy and neurodegeneration”. Curr Opin Neurobiol. 2018 Feb;48:153-159. doi: 10.1016/j.conb.2017.12.018. Epub 2018 Jan 6. PMID: 29316491.

Beacham GM, Partlow EA, Hollopeter G. “Conformational regulation of AP1 and AP2 clathrin adaptor complexes”. Traffic. 2019 Oct;20(10):741-751. doi: 10.1111/tra.12677. Epub 2019 Aug 6. PMID: 31313456; PMCID: PMC6774827.

Bera S, Camblor-Perujo S, Calleja Barca E, Negrete-Hurtado A, Racho J, De Bruyckere E, Wittich C, Ellrich N, Martins S, Adjaye J, Kononenko NL. “AP-2 reduces amyloidogenesis by promoting BACE1 trafficking and degradation in neurons”. EMBO Rep. 2020 Jun 4;21(6):e47954. doi: 10.15252/embr.201947954. Epub 2020 Apr 23. PMID: 32323475; PMCID: PMC7271323.

Berger Z, Roder H, Hanna A, Carlson A, Rangachari V, Yue M, Wszolek Z, Ashe K, Knight J, Dickson D, Andorfer C, Rosenberry TL, Lewis J, Hutton M, Janus C. “Accumulation of pathological tau species and memory loss in a conditional model of tauopathy”. J Neurosci. 2007 Apr 4;27(14):3650-62. doi: 10.1523/JNEUROSCI.0587-07.2007. PMID: 17409229; PMCID: PMC6672413.

Bernocco S, Fondelli C, Matteoni S, Magnoni L, Gotta S, Terstappen GC, Raggiaschi R. “Sequential detergent fractionation of primary neurons for proteomics studies”. Proteomics. 2008 Mar;8(5):930-8. doi: 10.1002/pmic.200700738. PMID: 18219698.

Bingol B. “Autophagy and lysosomal pathways in nervous system disorders”. Mol Cell Neurosci. 2018 Sep;91:167-208. doi: 10.1016/j.mcn.2018.04.009. Epub 2018 May 3. PMID: 29729319.

Bjørkøy G, Lamark T, Pankiv S, Øvervatn A, Brech A, Johansen T. Monitoring autophagic degradation of p62/SQSTM1. Methods Enzymol. 2009;452:181-97. doi: 10.1016/S0076-6879(08)03612-4. PMID: 19200883.

Boland B, Kumar A, Lee S, Platt FM, Wegiel J, Yu WH, Nixon RA. “Autophagy induction and autophagosome clearance in neurons: relationship to autophagic pathology in Alzheimer's disease”. J Neurosci. 2008 Jul 2;28(27):6926-37. doi: 10.1523/JNEUROSCI.0800-08.2008. PMID: 18596167; PMCID: PMC2676733.

Camblor-Perujo S, Kononenko NL. “Brain-specific functions of the endocytic machinery”. FEBS J. 2021 Apr 25. doi: 10.1111/febs.15897. Epub ahead of print. PMID: 33896112.

Cao Y, Xiao Y, Ravid R, Guan ZZ. « Changed clathrin regulatory proteins in the brains of Alzheimer's disease patients and animal models”. J Alzheimers Dis. 2010;22(1):329-42. doi: 10.3233/JAD-2010-100162. PMID: 20847448.

Ceccarelli B, Hurlbut WP, Mauro A. “Depletion of vesicles from frog neuromuscular junctions by prolonged tetanic stimulation”. J Cell Biol. 1972 Jul;54(1):30-8. doi: 10.1083/jcb.54.1.30. PMID: 4338962; PMCID: PMC2108853.

Cheng XT, Xie YX, Zhou B, Huang N, Farfel-Becker T, Sheng ZH. “Characterization of LAMP1-labeled nondegradative lysosomal and endocytic compartments in neurons”. J Cell Biol. 2018 Sep 3;217(9):3127-3139. doi: 10.1083/jcb.201711083. Epub 2018 Apr 25. PMID: 29695488; PMCID: PMC6123004.

Cheng XT, Zhou B, Lin MY, Cai Q, Sheng ZH. “Axonal autophagosomes recruit dynein for retrograde transport through fusion with late endosomes”. J Cell Biol. 2015 May 11;209(3):377-86. doi: 10.1083/jcb.201412046. Epub 2015 May 4. PMID: 25940348; PMCID: PMC4427784.

Cheung G, Cousin MA. “Synaptic vesicle generation from activity-dependent bulk endosomes requires calcium and calcineurin”. J Neurosci. 2013 Feb 20;33(8):3370-9. doi: 10.1523/JNEUROSCI.4697-12.2013. PMID: 23426665; PMCID: PMC3589713.

Ciechanover A, Brundin P. “The ubiquitin proteasome system in neurodegenerative diseases: sometimes the chicken, sometimes the egg”. Neuron. 2003 Oct 9;40(2):427-46. doi: 10.1016/s0896-6273(03)00606-8. PMID: 14556719.

Collins BM, McCoy AJ, Kent HM, Evans PR, Owen DJ. “Molecular architecture and functional model of the endocytic AP2 complex”. Cell. 2002 May 17;109(4):523-35. doi: 10.1016/s0092-8674(02)00735-3. PMID: 12086608.

Debnath J, Baehrecke EH, Kroemer G. “Does autophagy contribute to cell death?” Autophagy. 2005 Jul;1(2):66-74. doi: 10.4161/auto.1.2.1738. Epub 2005 Jul 13. PMID: 16874022.

Du J, Liang Y, Xu F, Sun B, Wang Z. “Trehalose rescues Alzheimer's disease phenotypes in APP/PS1 transgenic mice”. J Pharm Pharmacol. 2013 Dec;65(12):1753-6. doi: 10.1111/jphp.12108. Epub 2013 Aug 5. PMID: 24236985.

Feng T, Tammineni P, Agrawal C, Jeong YY, Cai Q. “Autophagy-mediated Regulation of BACE1 Protein Trafficking and Degradation”. J Biol Chem. 2017 Feb 3;292(5):1679-1690. doi: 10.1074/jbc.M116.766584. Epub 2016 Dec 27. PMID: 28028177; PMCID: PMC5290944.

Ferguson SM, Brasnjo G, Hayashi M, Wölfel M, Collesi C, Giovedi S, Raimondi A, Gong LW, Ariel P, Paradise S, O'toole E, Flavell R, Cremona O, Miesenböck G, Ryan TA, De Camilli P. “A selective activity-dependent requirement for dynamin 1 in synaptic vesicle endocytosis”. Science. 2007 Apr 27;316(5824):570-4. doi: 10.1126/science.1140621. PMID: 17463283.

Fernandes, A.C., V. Uytterhoeven, S. Kuenen, Y.C. Wang, J.R. Slabbaert, J. Swerts, J. Kasprowicz, S. Aerts, and P. Verstreken. 2014. “Reduced synaptic vesicle protein degradation at lysosomes curbs TBC1D24/sky-induced neurodegeneration”. J. Cell Biol. 207:453–462.

Frake RA, Ricketts T, Menzies FM, Rubinsztein DC. “Autophagy and neurodegeneration. J Clin Invest. 2015 Jan;125(1):65-74”. doi: 10.1172/JCI73944. Epub 2015 Jan 2. PMID: 25654552; PMCID: PMC4382230.

Fujikake N, Shin M, Shimizu S. “Association Between Autophagy and Neurodegenerative Diseases”. Front Neurosci. 2018 May 22;12:255. doi: 10.3389/fnins.2018.00255. PMID: 29872373; PMCID: PMC5972210.

Glatigny M, Moriceau S, Rivagorda M, Ramos-Brossier M, Nascimbeni AC, Lante F, Shanley MR, Boudarene N, Rousseaud A, Friedman AK, Settembre C, Kuperwasser N, Friedlander G, Buisson A, Morel E, Codogno P, Oury F. “Autophagy Is Required for Memory Formation and Reverses Age-Related Memory Decline”. Curr Biol. 2019 Feb 4;29(3):435-448.e8. doi: 10.1016/j.cub.2018.12.021. Epub 2019 Jan 17. PMID:

30661803.

Gouras GK, Tsai J, Naslund J, Vincent B, Edgar M, Checler F, Greenfield JP, Haroutunian V, Buxbaum JD, Xu H, Greengard P, Relkin NR. “Intraneuronal Abeta42 accumulation in human brain”. Am J Pathol. 2000 Jan;156(1):15-20. doi: 10.1016/s0002-9440(10)64700-1. PMID: 10623648; PMCID: PMC1868613.

Gutierrez MG, Munafó DB, Berón W, Colombo MI. “Rab7 is required for the normal progression of the autophagic pathway in mammalian cells”. J Cell Sci. 2004 Jun 1;117(Pt 13):2687-97. doi: 10.1242/jcs.01114. Epub 2004 May 11. PMID: 15138286.

Hara T, Nakamura K, Matsui M, Yamamoto A, Nakahara Y, Suzuki-Migishima R, Yokoyama M, Mishima K, Saito I, Okano H, Mizushima N. “Suppression of basal autophagy in neural cells causes neurodegenerative disease in mice”. Nature. 2006 Jun 15;441(7095):885-9. doi: 10.1038/nature04724. Epub 2006 Apr 19. PMID: 16625204.

He C, Klionsky DJ. “Regulation mechanisms and signaling pathways of autophagy”. Annu Rev Genet. 2009;43:67-93. doi: 10.1146/annurev-genet-102808-114910. PMID: 19653858; PMCID: PMC2831538.

Hemelaar J, Lelyveld VS, Kessler BM, Ploegh HL. “A single protease, Apg4B, is specific for the autophagy-related ubiquitin-like proteins GATE-16, MAP1-LC3, GABARAP, and Apg8L”. J Biol Chem. 2003 Dec 19;278(51):51841-50. doi: 10.1074/jbc.M308762200. Epub 2003 Oct 6. PMID: 14530254.

Hernandez D, Torres CA, Setlik W, Cebrián C, Mosharov EV, Tang G, Cheng HC, Kholodilov N, Yarygina O, Burke RE, Gershon M, Sulzer D. “Regulation of presynaptic neurotransmission by macroautophagy”. Neuron. 2012 Apr 26;74(2):277-84. doi: 10.1016/j.neuron.2012.02.020. PMID: 22542182; PMCID: PMC3578406.

Hill SE, Colón-Ramos DA. “The Journey of the Synaptic Autophagosome: A Cell Biological Perspective”. Neuron. 2020 Mar 18;105(6):961-973. doi: 10.1016/j.neuron.2020.01.018. PMID: 32191859.

Huynh KK, Eskelinen EL, Scott CC, Malevanets A, Saftig P, Grinstein S. “LAMP proteins are required for fusion of lysosomes with phagosomes”. EMBO J. 2007 Jan 24;26(2):313-24. doi: 10.1038/sj.emboj.7601511. PMID: 17245426; PMCID: PMC1783450.

Inobe T, Matouschek A. “Paradigms of protein degradation by the proteasome”. Curr Opin Struct Biol. 2014 Feb;24:156-64. doi: 10.1016/j.sbi.2014.02.002. Epub 2014 Mar 14. PMID: 24632559; PMCID: PMC4010099.

Inoki K, Kim J, Guan KL. “AMPK and mTOR in cellular energy homeostasis and drug targets”. Annu Rev Pharmacol Toxicol. 2012;52:381-400. doi: 10.1146/annurev-pharmtox-010611-134537. Epub 2011 Oct 17. PMID: 22017684.

Jiang T, Yu JT, Zhu XC, Tan MS, Wang HF, Cao L, Zhang QQ, Shi JQ, Gao L, Qin H, Zhang YD, Tan L. “Temsirolimus promotes autophagic clearance of amyloid-β and provides protective effects in cellular and animal models of Alzheimer's disease”. Pharmacol Res. 2014 Mar;81:54-63. doi: 10.1016/j.phrs.2014.02.008. Epub 2014 Mar 3. PMID: 24602800.

Johansen T, Lamark T. “Selective autophagy mediated by autophagic adapter proteins”. Autophagy. 2011 Mar;7(3):279-96. doi: 10.4161/auto.7.3.14487. PMID: 21189453; PMCID: PMC3060413.

Jung CH, Ro SH, Cao J, Otto NM, Kim DH. “mTOR regulation of autophagy”. FEBS Lett. 2010 Apr 2;584(7):1287-95. doi: 10.1016/j.febslet.2010.01.017. Epub 2010 Jan 18. PMID: 20083114; PMCID: PMC2846630.

Kirchhausen T, Owen D, Harrison SC. “Molecular structure, function, and dynamics of clathrin-mediated membrane traffic”. Cold Spring Harb Perspect Biol. 2014 May 1;6(5):a016725. doi: 10.1101/cshperspect.a016725. PMID: 24789820; PMCID: PMC3996469.

Klionsky DJ, Emr SD. “Autophagy as a regulated pathway of cellular degradation”. Science. 2000 Dec 1;290(5497):1717-21. doi: 10.1126/science.290.5497.1717. PMID: 11099404; PMCID: PMC2732363.

Knecht E, Aguado C, Cárcel J, Esteban I, Esteve JM, Ghislat G, Moruno JF, Vidal JM, Sáez R. “Intracellular protein degradation in mammalian cells: recent developments”. Cell Mol Life Sci. 2009 Aug;66(15):2427-43. doi: 10.1007/s00018-009-0030-6. Epub 2009 Apr 28. PMID: 19399586.

Komatsu M, Waguri S, Chiba T, Murata S, Iwata J, Tanida I, Ueno T, Koike M, Uchiyama Y, Kominami E, Tanaka K. “Loss of autophagy in the central nervous system causes neurodegeneration in mice”. Nature. 2006 Jun 15;441(7095):880-4. doi: 10.1038/nature04723. Epub 2006 Apr 19. PMID: 16625205.

Komatsu M, Waguri S, Koike M, Sou YS, Ueno T, Hara T, Mizushima N, Iwata J, Ezaki

J, Murata S, Hamazaki J, Nishito Y, Iemura S, Natsume T, Yanagawa T, Uwayama J, Warabi E, Yoshida H, Ishii T, Kobayashi A, Yamamoto M, Yue Z, Uchiyama Y, Kominami E, Tanaka K. “Homeostatic levels of p62 control cytoplasmic inclusion body formation in autophagy-deficient mice”. Cell. 2007 Dec 14;131(6):1149-63. doi: 10.1016/j.cell.2007.10.035. PMID: 18083104.

Kononenko NL, Claßen GA, Kuijpers M, Puchkov D, Maritzen T, Tempes A, Malik AR, Skalecka A, Bera S, Jaworski J, Haucke V. “Retrograde transport of TrkB-containing autophagosomes via the adaptor AP-2 mediates neuronal complexity and prevents neurodegeneration”. Nat Commun. 2017 Apr 7;8:14819. doi: 10.1038/ncomms14819. PMID: 28387218; PMCID: PMC5385568.

Kononenko NL, Haucke V. “Molecular mechanisms of presynaptic membrane retrieval and synaptic vesicle reformation”. Neuron. 2015 Feb 4;85(3):484-96. doi: 10.1016/j.neuron.2014.12.016. PMID: 25654254.

Kononenko NL, Puchkov D, Classen GA, Walter AM, Pechstein A, Sawade L, Kaempf N, Trimbuch T, Lorenz D, Rosenmund C, Maritzen T, Haucke V. “Clathrin/AP-2 mediate synaptic vesicle reformation from endosome-like vacuoles but are not essential for membrane retrieval at central synapses”. Neuron. 2014 Jun 4;82(5):981-8. doi: 10.1016/j.neuron.2014.05.007. PMID: 24908483.

Koukourakis MI, Kalamida D, Giatromanolaki A, Zois CE, Sivridis E, Pouliliou S, Mitrakas A, Gatter KC, Harris AL. “Autophagosome Proteins LC3A, LC3B and LC3C Have Distinct Subcellular Distribution Kinetics and Expression in Cancer Cell Lines”. PLoS One. 2015 Sep 17;10(9):e0137675. doi: 10.1371/journal.pone.0137675. PMID: 26378792; PMCID: PMC4574774.

Kraft C, Kijanska M, Kalie E, Siergiejuk E, Lee SS, Semplicio G, Stoffel I, Brezovich A, Verma M, Hansmann I, Ammerer G, Hofmann K, Tooze S, Peter M. “Binding of the Atg1/ULK1 kinase to the ubiquitin-like protein Atg8 regulates autophagy”. EMBO J. 2012 Sep 12;31(18):3691-703. doi: 10.1038/emboj.2012.225. Epub 2012 Aug 10. PMID: 22885598; PMCID: PMC3442273.

Krüger U, Wang Y, Kumar S, Mandelkow EM. “Autophagic degradation of tau in primary neurons and its enhancement by trehalose”. Neurobiol Aging. 2012 Oct;33(10):2291-305. doi: 10.1016/j.neurobiolaging.2011.11.009. Epub 2011 Dec 14. PMID: 22169203.

Kulkarni VV, Maday S. “Compartment-specific dynamics and functions of autophagy in neurons”. Dev Neurobiol. 2018a Mar;78(3):298-310. doi: 10.1002/dneu.22562. Epub 2017 Dec 15. PMID: 29197160; PMCID: PMC5816696.

Kulkarni VV, Maday S. “Neuronal endosomes to lysosomes: A journey to the soma”. J Cell Biol. 2018b Sep 3;217(9):2977-2979. doi: 10.1083/jcb.201806139. Epub 2018b Aug 16. PMID: 30115668; PMCID: PMC6123003.

Laemmli UK. “Cleavage of structural proteins during the assembly of the head of bacteriophage T4”. Nature. 1970 Aug 15;227(5259):680-5. doi: 10.1038/227680a0. PMID: 5432063.

Lamb CA, Yoshimori T, Tooze SA. The autophagosome: origins unknown, biogenesis complex. Nat Rev Mol Cell Biol. 2013 Dec;14(12):759-74. doi: 10.1038/nrm3696. Epub 2013 Nov 8. PMID: 24201109.

Lee JH, Yu WH, Kumar A, Lee S, Mohan PS, Peterhoff CM, Wolfe DM, Martinez-Vicente M, Massey AC, Sovak G, Uchiyama Y, Westaway D, Cuervo AM, Nixon RA. “Lysosomal proteolysis and autophagy require presenilin 1 and are disrupted by Alzheimer-related PS1 mutations”. Cell. 2010 Jun 25;141(7):1146-58. doi: 10.1016/j.cell.2010.05.008. Epub 2010 Jun 10. PMID: 20541250; PMCID: PMC3647462.

Levine B, Klionsky DJ. “Development by self-digestion: molecular mechanisms and biological functions of autophagy”. Dev Cell. 2004 Apr;6(4):463-77. doi: 10.1016/s1534-5807(04)00099-1. PMID: 15068787.

Lilienbaum A. “Relationship between the proteasomal system and autophagy”. Int J Biochem Mol Biol. 2013 Mar 31;4(1):1-26. PMID: 23638318; PMCID: PMC3627065.

Livneh I, Cohen-Kaplan V, Avni N, Fabre B, Ziv T, Kwon YT, Ciechanover A. “p62- and ubiquitin-dependent stress-induced autophagy of the mammalian 26S proteasome”. Proc Natl Acad Sci U S A. 2016 Nov 22;113(47):E7490-E7499. doi: 10.1073/pnas.1615455113. Epub 2016 Oct 17. PMID: 27791183; PMCID: PMC5127335.

Long JM, Holtzman DM. “Alzheimer Disease: An Update on Pathobiology and Treatment Strategies”. Cell. 2019 Oct 3;179(2):312-339. doi: 10.1016/j.cell.2019.09.001. Epub 2019 Sep 26. PMID: 31564456; PMCID: PMC6778042.

Longatti A, Tooze SA. “Vesicular trafficking and autophagosome formation”. Cell Death Differ. 2009 Jul;16(7):956-65. doi: 10.1038/cdd.2009.39. Epub 2009 Apr 17. PMID: 19373247.

Maday S, Holzbaur EL. “Autophagosome biogenesis in primary neurons follows an ordered and spatially regulated pathway.” Dev Cell. 2014 Jul 14;30(1):71-85. doi: 10.1016/j.devcel.2014.06.001. PMID: 25026034; PMCID: PMC4109719.

Maday S, Holzbaur EL. Compartment-Specific Regulation of Autophagy in Primary Neurons. J Neurosci. 2016 Jun 1;36(22):5933-45. doi: 10.1523/JNEUROSCI.4401-15.2016. PMID: 27251616; PMCID: PMC4887563.

Maday S, Wallace KE, Holzbaur EL. Autophagosomes initiate distally and mature during transport toward the cell soma in primary neurons. J Cell Biol. 2012 Feb 20;196(4):407-17. doi: 10.1083/jcb.201106120. Epub 2012 Feb 13. PMID: 22331844; PMCID: PMC3283992.

Masliah E, Mallory M, Alford M, DeTeresa R, Hansen LA, McKeel DW Jr, Morris JC. Altered expression of synaptic proteins occurs early during progression of Alzheimer's disease. Neurology. 2001 Jan 9;56(1):127-9. doi: 10.1212/wnl.56.1.127. PMID: 11148253.

McMahon HT, Boucrot E. “Molecular mechanism and physiological functions of clathrin-mediated endocytosis”. Nat Rev Mol Cell Biol. 2011 Jul 22;12(8):517-33. doi: 10.1038/nrm3151. PMID: 21779028.

Menzies FM, Fleming A, Rubinsztein DC. “Compromised autophagy and neurodegenerative diseases”. Nat Rev Neurosci. 2015 Jun;16(6):345-57. doi: 10.1038/nrn3961. PMID: 25991442.

Mindell JA. “Lysosomal acidification mechanisms”. Annu Rev Physiol. 2012;74:69-86. doi: 10.1146/annurev-physiol-012110-142317. PMID: 22335796.

Mizushima N, Murphy LO. “Autophagy Assays for Biological Discovery and Therapeutic Development”. Trends Biochem Sci. 2020 Dec;45(12):1080-1093. doi: 10.1016/j.tibs.2020.07.006. Epub 2020 Aug 21. PMID: 32839099.

Mizushima N. “Autophagy: process and function”. Genes Dev. 2007 Nov 15;21(22):2861-73. doi: 10.1101/gad.1599207. PMID: 18006683.

Mizushima N. “The ATG conjugation systems in autophagy”. Curr Opin Cell Biol. 2020 Apr;63:1-10. doi: 10.1016/j.ceb.2019.12.001. Epub 2019 Dec 31. PMID: 31901645.

Murdoch JD, Rostosky CM, Gowrisankaran S, Arora AS, Soukup SF, Vidal R, Capece V, Freytag S, Fischer A, Verstreken P, Bonn S, Raimundo N, Milosevic I. “Endophilin-A deficiency induces the Foxo3a-Fbxo32 network in the brain and causes dysregulation of autophagy and the ubiquitin-proteasome system”. Cell Rep. 2016 Oct 18;17(4):1071-1086. doi: 10.1016/j.celrep.2016.09.058. Epub 2016 Oct 6. PMID: 27720640; PMCID: PMC5080600.

Nakatogawa H. “Mechanisms governing autophagosome biogenesis”. Nat Rev Mol Cell Biol. 2020 Aug;21(8):439-458. doi: 10.1038/s41580-020-0241-0. Epub 2020 May 5. PMID: 32372019.

Nazarko VY, Zhong Q. “ULK1 targets Beclin-1 in autophagy”. Nat Cell Biol. 2013 Jul;15(7):727-8. doi: 10.1038/ncb2797. PMID: 23817237; PMCID: PMC4442023.

Nilsson P, Loganathan K, Sekiguchi M, Matsuba Y, Hui K, Tsubuki S, Tanaka M, Iwata N, Saito T, Saido TC. “Aβ secretion and plaque formation depend on autophagy”. Cell Rep. 2013 Oct 17;5(1):61-9. doi: 10.1016/j.celrep.2013.08.042. Epub 2013 Oct 3. PMID: 24095740.

Nixon RA, Yang DS. “Autophagy failure in Alzheimer's disease - locating the primary defect”. Neurobiol Dis. 2011 Jul;43(1):38-45. doi: 10.1016/j.nbd.2011.01.021. Epub 2011 Feb 3. PMID: 21296668; PMCID: PMC3096679.

Nixon RA. “The role of autophagy in neurodegenerative disease.” Nat Med. 2013 Aug;19(8):983-97. doi: 10.1038/nm.3232. Epub 2013 Aug 6. PMID: 23921753.

Okerlund ND, Schneider K, Leal-Ortiz S, Montenegro-Venegas C, Kim SA, Garner LC, Waites CL, Gundelfinger ED, Reimer RJ, Garner CC. “Bassoon Controls Presynaptic Autophagy through Atg5. Neuron”. 2017 Feb 22;93(4):897-913.e7. doi: 10.1016/j.neuron.2017.01.026. Erratum in: Neuron. 2018 Feb 7;97(3):727. PMID: 28231469.

Overhoff M, De Bruyckere E, Kononenko NL. “Mechanisms of neuronal survival safeguarded by endocytosis and autophagy”. J Neurochem. 2021 Apr;157(2):263-296. doi: 10.1111/jnc.15194. Epub 2020 Oct 21. PMID: 32964462.

Parzych KR, Klionsky DJ. An overview of autophagy: morphology, mechanism, and regulation. Antioxid Redox Signal. 2014 Jan 20;20(3):460-73. doi: 10.1089/ars.2013.5371. Epub 2013 Aug 2. PMID: 23725295; PMCID: PMC3894687.

Piccini A, Castroflorio E, Valente P, Guarnieri FC, Aprile D, Michetti C, Bramini M, Giansante G, Pinto B, Savardi A, Cesca F, Bachi A, Cattaneo A, Wren JD, Fassio A,

Valtorta F, Benfenati F, Giovedì S. “APache is an AP2-interacting protein involved in synaptic vesicle trafficking and neuronal development”. Cell Rep. 2017 Dec 19;21(12):3596-3611. doi: 10.1016/j.celrep.2017.11.073. PMID: 29262337.

Piccini A, Perlini LE, Cancedda L, Benfenati F, Giovedì S. “Phosphorylation by PKA and Cdk5 Mediates the Early Effects of Synapsin III in Neuronal Morphological Maturation”. J Neurosci. 2015 Sep 23;35(38):13148-59. doi: 10.1523/JNEUROSCI.1379-15.2015. PMID: 26400944; PMCID: PMC6605445.

Reef S, Zalckvar E, Shifman O, Bialik S, Sabanay H, Oren M, Kimchi A. “A short mitochondrial form of p19ARF induces autophagy and caspase-independent cell death”. Mol Cell. 2006 May 19;22(4):463-75. doi: 10.1016/j.molcel.2006.04.014. PMID: 16713577.

Roberts R. “Lysosomal cysteine proteases: structure, function and inhibition of cathepsins”. Drug News Perspect. 2005 Dec;18(10):605-14. doi: 10.1358/dnp.2005.18.10.949485. PMID: 16491162.

Rodríguez-Martín T, Cuchillo-Ibáñez I, Noble W, Nyenya F, Anderton BH, Hanger DP. « Tau phosphorylation affects its axonal transport and degradation”. Neurobiol Aging. 2013 Sep;34(9):2146-57. doi: 10.1016/j.neurobiolaging.2013.03.015. Epub 2013 Apr 17. PMID: 23601672; PMCID: PMC3684773.

Rubinsztein DC, Mariño G, Kroemer G. “Autophagy and aging”. Cell. 2011 Sep 2;146(5):682-95. doi: 10.1016/j.cell.2011.07.030. PMID: 21884931.

Russell RC, Tian Y, Yuan H, Park HW, Chang YY, Kim J, Kim H, Neufeld TP, Dillin A, Guan KL. “ULK1 induces autophagy by phosphorylating Beclin-1 and activating VPS34 lipid kinase”. Nat Cell Biol. 2013 Jul;15(7):741-50. doi: 10.1038/ncb2757. Epub 2013 May 19. PMID: 23685627; PMCID: PMC3885611.

Ryter SW, Cloonan SM, Choi AM. “Autophagy: a critical regulator of cellular metabolism and homeostasis”. Mol Cells. 2013 Jul;36(1):7-16. doi: 10.1007/s10059-013-0140-8. Epub 2013 May 24. PMID: 23708729; PMCID: PMC3887921.

Saftig P, Klumperman J. “Lysosome biogenesis and lysosomal membrane proteins: trafficking meets function”. Nat Rev Mol Cell Biol. 2009 Sep;10(9):623-35. doi: 10.1038/nrm2745. Epub 2009 Aug 12. PMID: 19672277.

Satoo K, Noda NN, Kumeta H, Fujioka Y, Mizushima N, Ohsumi Y, Inagaki F. “The structure of Atg4B-LC3 complex reveals the mechanism of LC3 processing and

delipidation during autophagy". EMBO J. 2009 May 6;28(9):1341-50. doi: 10.1038/emboj.2009.80. Epub 2009 Mar 26. PMID: 19322194; PMCID: PMC2683054.

Shpilka T, Weidberg H, Pietrokovski S, Elazar Z. "Atg8: an autophagy-related ubiquitin-like protein family". Genome Biol. 2011 Jul 27;12(7):226. doi: 10.1186/gb-2011-12-7-226. PMID: 21867568; PMCID: PMC3218822.

Soukup SF, Kuenen S, Vanhauwaert R, Manetsberger J, Hernández-Díaz S, Swerts J, Schoovaerts N, Vilain S, Gounko NV, Vints K, Geens A, De Strooper B, Verstreken P. "A LRRK2-dependent endophilin-A phosphoswitch is critical for macroautophagy at presynaptic terminals". Neuron. 2016 Nov 23;92(4):829-844. doi: 10.1016/j.neuron.2016.09.037. Epub 2016 Oct 6. PMID: 27720484.

Soykan T, Maritzen T, Haucke V. "Modes and mechanisms of synaptic vesicle recycling. Curr Opin Neurobiol". 2016 Aug;39:17-23. doi: 10.1016/j.conb.2016.03.005. Epub 2016 Mar 24. PMID: 27016897.

Spilman P, Podlutskaya N, Hart MJ, Debnath J, Gorostiza O, Bredesen D, Richardson A, Strong R, Galvan V. "Inhibition of mTOR by rapamycin abolishes cognitive deficits and reduces amyloid-beta levels in a mouse model of Alzheimer's disease". PLoS One. 2010 Apr 1;5(4):e9979. doi: 10.1371/journal.pone.0009979. Erratum in: PLoS One. 2011;6(11). doi:10.1371/annotation/05c1b976-7eab-4154-808d-0526e604b8eb. PMID: 20376313; PMCID: PMC2848616.

Suzuki K, Ohsumi Y. "Current knowledge of the pre-autophagosomal structure (PAS)". FEBS Lett. 2010 Apr 2;584(7):1280-6. doi: 10.1016/j.febslet.2010.02.001. Epub 2010 Feb 5. PMID: 20138172.

Takahashi RH, Milner TA, Li F, Nam EE, Edgar MA, Yamaguchi H, Beal MF, Xu H, Greengard P, Gouras GK. "Intraneuronal Alzheimer abeta42 accumulates in multivesicular bodies and is associated with synaptic pathology". Am J Pathol. 2002 Nov;161(5):1869-79. doi: 10.1016/s0002-9440(10)64463-x. PMID: 12414533; PMCID: PMC1850783.

Takei K, Mundigl O, Daniell L, De Camilli P. "The synaptic vesicle cycle: a single vesicle budding step involving clathrin and dynamin". J Cell Biol. 1996 Jun;133(6):1237-50. doi: 10.1083/jcb.133.6.1237. PMID: 8682861; PMCID: PMC2120898.

Tammineni P, Ye X, Feng T, Aikal D, Cai Q. "Impaired retrograde transport of axonal autophagosomes contributes to autophagic stress in Alzheimer's disease neurons".

Elife. 2017 Jan 13;6:e21776. doi: 10.7554/eLife.21776. PMID: 28085665; PMCID: PMC5235353.

Tanaka K. “The proteasome: overview of structure and functions”. Proc Jpn Acad Ser B Phys Biol Sci. 2009;85(1):12-36. doi: 10.2183/pjab.85.12. PMID: 19145068; PMCID: PMC3524306.

Tian Y, Chang JC, Fan EY, Flajolet M, Greengard P. “Adaptor complex AP2/PICALM, through interaction with LC3, targets Alzheimer's APP-CTF for terminal degradation via autophagy”. Proc Natl Acad Sci U S A. 2013 Oct 15;110(42):17071-6. doi: 10.1073/pnas.1315110110. Epub 2013 Sep 25. PMID: 24067654; PMCID: PMC3801056.

Trivedi PC, Bartlett JJ, Pulinilkunnil T. “Lysosomal Biology and Function: Modern View of Cellular Debris Bin”. Cells. 2020 May 4;9(5):1131. doi: 10.3390/cells9051131. PMID: 32375321; PMCID: PMC7290337.

Tsukada M, Ohsumi Y. “Isolation and characterization of autophagy-defective mutants of Saccharomyces cerevisiae”. FEBS Lett. 1993 Oct 25;333(1-2):169-74. doi: 10.1016/0014-5793(93)80398-e. PMID: 8224160.

Uytterhoeven V, Kuenen S, Kasprowicz J, Miskiewicz K, Verstreken P. “Loss of skywalker reveals synaptic endosomes as sorting stations for synaptic vesicle proteins”. Cell. 2011 Apr 1;145(1):117-32. doi: 10.1016/j.cell.2011.02.039. PMID: 21458671.

Vijayan V, Verstreken P. “Autophagy in the presynaptic compartment in health and disease”. J Cell Biol. 2017 Jul 3;216(7):1895-1906. doi: 10.1083/jcb.201611113. Epub 2017 May 17. PMID: 28515275; PMCID: PMC5496617.

Wang CW, Klionsky DJ. “The molecular mechanism of autophagy”. Mol Med. 2003 Mar-Apr;9(3-4):65-76. PMID: 12865942; PMCID: PMC1430730.

Wang D, Chan CC, Cherry S, Hiesinger PR. “Membrane trafficking in neuronal maintenance and degeneration”. Cell Mol Life Sci. 2013 Aug;70(16):2919-34. doi: 10.1007/s00018-012-1201-4. Epub 2012 Nov 8. PMID: 23132096; PMCID: PMC3722462.

Wang T, Martin S, Papadopulos A, Harper CB, Mavlyutov TA, Niranjan D, Glass NR, Cooper-White JJ, Sibarita JB, Choquet D, Davletov B, Meunier FA. “Control of autophagosome axonal retrograde flux by presynaptic activity unveiled using botulinum

neurotoxin type a". J Neurosci. 2015 Apr 15;35(15):6179-94. doi: 10.1523/JNEUROSCI.3757-14.2015. PMID: 25878289; PMCID: PMC4787026.

Wang Y, Zhang H. "Regulation of Autophagy by mTOR Signaling Pathway". Adv Exp Med Biol. 2019;1206:67-83. doi: 10.1007/978-981-15-0602-4_3. PMID: 31776980.

Wang YC, Lauwers E, Verstreken P. "Presynaptic protein homeostasis and neuronal function". Curr Opin Genet Dev. 2017 Jun;44:38-46. doi: 10.1016/j.gde.2017.01.015. Epub 2017 Feb 16. PMID: 28213157.

Watanabe S, Liu Q, Davis MW, Hollopeter G, Thomas N, Jorgensen NB, Jorgensen EM. "Ultrafast endocytosis at Caenorhabditis elegans neuromuscular junctions". Elife. 2013a Sep 3;2:e00723. doi: 10.7554/eLife.00723. PMID: 24015355; PMCID: PMC3762212.

Watanabe S, Rost BR, Camacho-Pérez M, Davis MW, Söhl-Kielczynski B, Rosenmund C, Jorgensen EM. "Ultrafast endocytosis at mouse hippocampal synapses". Nature. 2013b Dec 12;504(7479):242-247. doi: 10.1038/nature12809. Epub 2013 Dec 4. PMID: 24305055; PMCID: PMC3957339.

Watanabe S, Trimbuch T, Camacho-Pérez M, Rost BR, Brokowski B, Söhl-Kielczynski B, Felies A, Davis MW, Rosenmund C, Jorgensen EM. "Clathrin regenerates synaptic vesicles from endosomes". Nature. 2014 Nov 13;515(7526):228-33. doi: 10.1038/nature13846. Epub 2014 Oct 8. PMID: 25296249; PMCID: PMC4291189.

Wertz MH, Mitchem MR, Pineda SS, Hachigian LJ, Lee H, Lau V, Powers A, Kulicke R, Madan GK, Colic M, Therrien M, Vernon A, Beja-Glasser VF, Hegde M, Gao F, Kellis M, Hart T, Doench JG, Heiman M. "Genome-wide In Vivo CNS Screening Identifies Genes that Modify CNS Neuronal Survival and mHTT Toxicity". Neuron. 2020 Apr 8;106(1):76-89.e8. doi: 10.1016/j.neuron.2020.01.004. Epub 2020 Jan 30. PMID: 32004439; PMCID: PMC7181458.

Whyte LS, Lau AA, Hemsley KM, Hopwood JJ, Sargeant TJ. "Endo-lysosomal and autophagic dysfunction: a driving factor in Alzheimer's disease?" J Neurochem. 2017 Mar;140(5):703-717. doi: 10.1111/jnc.13935. Epub 2017 Jan 23. PMID: 28027395.

Wirth M, Joachim J, Tooze SA. "Autophagosome formation - the role of ULK1 and Beclin1-PI3KC3 complexes in setting the stage". Semin Cancer Biol. 2013 Oct;23(5):301-9. doi: 10.1016/j.semcancer.2013.05.007. Epub 2013 May 29. PMID: 23727157.

Wong PM, Puente C, Ganley IG, Jiang X. “The ULK1 complex: sensing nutrient signals for autophagy activation”. Autophagy. 2013 Feb 1;9(2):124-37. doi: 10.4161/auto.23323. Epub 2013 Jan 7. PMID: 23295650; PMCID: PMC3552878.

Wren JD. “A global meta-analysis of microarray expression data to predict unknown gene functions and estimate the literature-data divide”. Bioinformatics. 2009 Jul 1;25(13):1694-701. doi: 10.1093/bioinformatics/btp290. Epub 2009 May 15. PMID: 19447786; PMCID: PMC2732319.

Yang Y, Kim J, Kim HY, Ryoo N, Lee S, Kim Y, Rhim H, Shin YK. “Amyloid-β Oligomers May Impair SNARE-Mediated Exocytosis by Direct Binding to Syntaxin 1a”. Cell Rep. 2015 Aug 25;12(8):1244-51. doi: 10.1016/j.celrep.2015.07.044. Epub 2015 Aug 13. PMID: 26279571; PMCID: PMC4955600.

Yang Z, Klionsky DJ. “Mammalian autophagy: core molecular machinery and signaling regulation”. Curr Opin Cell Biol. 2010 Apr;22(2):124-31. doi: 10.1016/j.ceb.2009.11.014. Epub 2009 Dec 23. PMID: 20034776; PMCID: PMC2854249.

Yao PJ, Zhu M, Pyun EI, Brooks AI, Therianos S, Meyers VE, Coleman PD. “Defects in expression of genes related to synaptic vesicle trafficking in frontal cortex of Alzheimer's disease”. Neurobiol Dis. 2003 Mar;12(2):97-109. doi: 10.1016/s0969-9961(02)00009-8. PMID: 12667465.

Yao PJ. “Synaptic frailty and clathrin-mediated synaptic vesicle trafficking in Alzheimer's disease”. Trends Neurosci. 2004 Jan;27(1):24-9. doi: 10.1016/j.tins.2003.10.012. PMID: 14698607.

Yap CC, Digilio L, McMahon LP, Garcia ADR, Winckler B. “Degradation of dendritic cargos requires Rab7-dependent transport to somatic lysosomes”. J Cell Biol. 2018 Sep 3;217(9):3141-3159. doi: 10.1083/jcb.201711039. Epub 2018 Jun 15. PMID: 29907658; PMCID: PMC6122995.

Ye X, Feng T, Tammineni P, Chang Q, Jeong YY, Margolis DJ, Cai H, Kusnecov A, Cai Q. “Regulation of Synaptic Amyloid-β Generation through BACE1 Retrograde Transport in a Mouse Model of Alzheimer's Disease”. J Neurosci. 2017 Mar 8;37(10):2639-2655. doi: 10.1523/JNEUROSCI.2851-16.2017. Epub 2017 Feb 3. PMID: 28159908; PMCID: PMC5354320.

# 9. Appendix

Papers published as coauthor by Barbara Parisi during the PhD course:

[REVIEW] Giovedì S, Ravanelli MM, **Parisi B**, Bettegazzi B, Guarnieri FC. "**Dysfunctional Autophagy and Endolysosomal System in Neurodegenerative Diseases: Relevance and Therapeutic Options**". Front Cell Neurosci. 2020 Dec 17;14:602116. doi: 10.3389/fncel.2020.602116. PMID: 33390907; PMCID: PMC7773602.

Rocchi A, Sacchetti S, De Fusco A, Giovedi S, **Parisi B**, Cesca F, Höltje M, Ruprecht K, Ahnert-Hilger G, Benfenati F. Correction: "**Autoantibodies to synapsin I sequestrate synapsin I and alter synaptic function**". Cell Death Dis. 2020 Jan 14;11(1):27. doi: 10.1038/s41419-019-2220-y. Erratum for: Cell Death Dis. 2019 Nov 14;10(11):864. PMID: 31937775; PMCID: PMC6960144.